EVERT NASEDKIN

SIMULATED INSTRUMENTAL CONSTRAINTS ON SUB-STELLAR ATMOSPHERIC RETRIEVALS FOR THE JAMES WEBB SPACE TELESCOPE'S MID-INFRARED INSTRUMENT.

Evert Nasedkin
Simulated Instrumental Constraints on Sub-Stellar Atmospheric Retrievals for the James Webb Space Telescope's Mid-Infrared Instrument.

TITLEBACK
This document was written with LaTeX on Ubuntu using ArsClassica, designed by André Miede.

CONTACTS
☞ evertn@student.ethz.ch

Eidgenössische Technische Hochschule Zürich
Swiss Federal Institute of Technology Zurich

Declaration of originality

The signed declaration of originality is a component of every semester paper, Bachelor's thesis, Master's thesis and any other degree paper undertaken during the course of studies, including the respective electronic versions.

Lecturers may also require a declaration of originality for other written papers compiled for their courses.

I hereby confirm that I am the sole author of the written work here enclosed and that I have compiled it in my own words. Parts excepted are corrections of form and content by the supervisor.

Title of work (in block letters):

Authored by (in block letters):
For papers written by groups the names of all authors are required.

Name(s): **First name(s):**

With my signature I confirm that
- I have committed none of the forms of plagiarism described in the 'Citation etiquette' information sheet.
- I have documented all methods, data and processes truthfully.
- I have not manipulated any data.
- I have mentioned all persons who were significant facilitators of the work.

I am aware that the work may be screened electronically for plagiarism.

Place, date **Signature(s)**

For papers written by groups the names of all authors are required. Their signatures collectively guarantee the entire content of the written paper.

ACKNOWLEDGEMENTS

—

ABSTRACT

Following its launch in 2021, the James Webb Telescope will provide the best infrared observations of exoplanets and brown dwarfs to date. In particular, the Mid-Infrared Instrument (MIRI), will allow for medium resolution spectroscopy across a wide wavelength band, from 4.9-28.8μm. This will allow us to derive atmospheric properties of objects at lower temperatures than currently possible. MIRI's medium resolution spectrometer (MRS) is an integrated field unit that will perform these observations, providing both spatial and spectral information about targets. Understanding the instrumental effects is critical to analyzing data from MIRI. With that in mind, the MIRISIM instrumental simulator was developed to provide observational simulations of the various sub instruments of MIRI.

This thesis improves the implementation of a thin-film fringing model for point sources to MIRISIM, considering how the fringing effect from the detector layers varies with position. Fringing is a periodic, wavelength dependent effect, and thus has a strong impact on any spectroscopic observations. A comparison to the existing model was made, demonstrating the necessity of considering this effect when analyzing data. We will improve the fringing removal by identifying the point source location from the constructed data cube, and select the correct fringe flat for removal.

Understanding the instrumental effects is key to quantifying the ability of MIRI to derive atmospheric properties. Existing literature has considered the NIRCAM instrument and the MIRI Low-Resolution Spectrometer, but to date no retrieval studies have been performed using MIRISIM, or for the MIRI MRS, though it is critical to extend wavelength coverage to improve the results of an atmospheric retrieval. Model atmospheres will be generated using PetitRadTrans, and processed using MIRISIM and the JWST pipeline to produce a mock observation. An atmospheric retrieval will be performed, demonstrating to what extent MIRI will be able to retrieve atmospheric parameters such as temperature, pressure and composition. The posterior distributions of these parameters are compared with and without the fringing removal, again demonstrating the importance of correcting for this effect.

CONTENTS

1 INTRODUCTION

Since the first detection of a planet around a sun-like star (Mayor et al., 1995) the field of exoplanets has evolved rapidly. Thousands of companions have been identified using the radial velocity and transit detection methods, and a handful have been imaged directly using both ground and space based observatories. In the last decade, many advances have been made that allow us to begin to characterize the properties of a few of these planets using spectroscopy. With the launch of the James Webb Space Telescope (JWST) in 2021, and the dawn of the era of extremely large telescopes, we will be able to peer deeper into these planets and further constrain atmospheric or geological properties, allowing us to answer questions about their formation history, climate, and even the prospects for habitability and life.

JWST will operate in near to mid infrared wavelengths, which will provide a new window into studying the atmospheres of exoplanets and brown dwarfs. The Mid Infrared Instrument (MIRI) will provide unprecedented spectral resolution in the mid infrared, allowing for the measurement of composition, pressure and temperature. Novel instrumentation does not come without challenges. Optical and instrumental effects will constrain the ability to which we can measure spectral features, which will ultimately limit the science that can be accomplished.

In this thesis, we will measure the impact of thin-film fringing in the layers of the detectors in the MIRI Medium-Resolution Spectrometer on measurements of atmospheric parameters of brown dwarfs and exoplanets. This will provide a baseline for determining the level of correction necessary to minimize the impact of fringing, as well as providing a first look into the ability of the MRS to characterize atmospheres.

1.1 EXOPLANETS

The last quarter century of observations has revealed the diversity of exoplanets and extra-solar systems. Both the architecture and individual planetary characteristics vary greatly when compared to each other, as well as to our own solar system. From the hot Jupiters initially found by Mayor and Queloz (Mayor et al., 1995) to the thousands of planets discovered by the Kepler mission, the variety in exoplanets has raised questions about their formation and development, as well as their present day structure, climate, and even prospects for life. Improvements to observational techniques have allowed us to improve our understanding of these planets. Secondary eclipse and transmission spectroscopy has opened the door to the study of planets in close orbits to their host stars, while emission spectroscopy of young planet has allowed for constraints on models of planet formation. Over the next decades, new instruments will be developed that improve sensitivity,

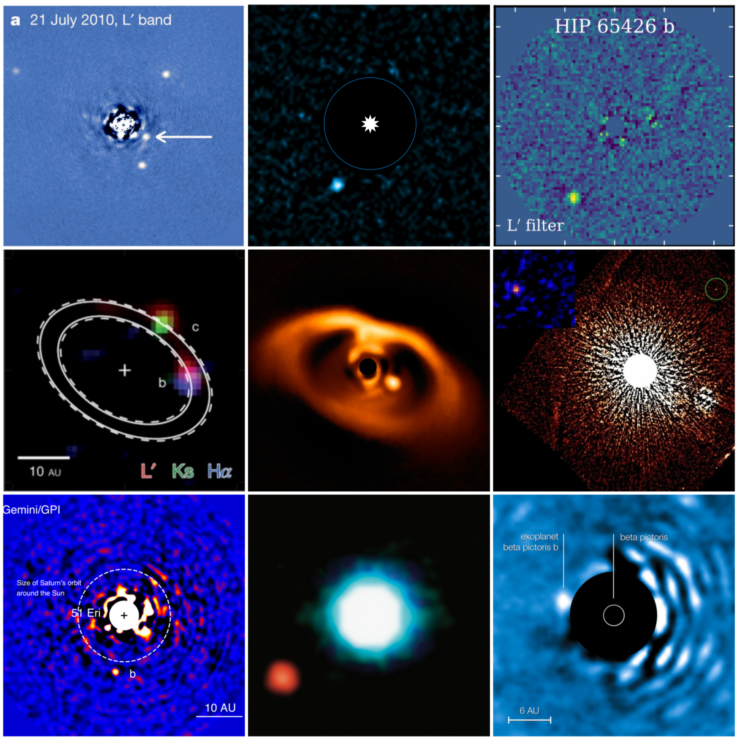

Figure 1: A family portrait of some of the directly imaged exoplanets. (**Marois2010**; **Rameau2013**; **Stolker2020**; **Sallum2015**; **Currie2018**; Chauvin et al., 2004; Keppler et al., 2018; Macintosh et al., 2015; Quanz et al., 2010).

allowing us to study smaller, colder and fainter planets: with the ultimate goal of studying atmospheric and surface features of an earth-like planet.

Of particular interest are observable features that allow us to measure physical properties of exoplanets. The radial velocity (RV) method provides a measure of the planet mass, while a transit can constrain the radius. Already these properties tell us something about the overall structure of the planet. Spectroscopy can provide insight into the composition of the planet's atmosphere, as well as its temperature and pressure. These properties are linked to its age and location of formation in the circumstellar disk. The atmosphere, combined with the distance between the planet and its star determine the climate of the planet.

Direct Imaging

While the majority of exoplanet detections have been made using the radial velocity or transit techniques, direct imaging opens up the possibility of collecting light from the planet itself. This provides a window into the planet's atmosphere and surface. Most direct imaging to date has used near-to-mid infrared wavelengths, where the contrast between the thermal emission from the planet and the star is at a minimum. This has its drawbacks: we are so far only able to image young planets that have retained some of the heat from their formation.

Direct imaging can make use of both ground and space based observatories. However, the high spatial resolution required drives the need for a large primary mirror, limiting the possibilities of space-based telescopes. On the other hand, atmospheric turbulence necessitates the use of an adaptive optics equipped facility to observe from the ground. Atmospheric absorption due to telluric lines (absorption lines of Earth's atmosphere) also restrict infrared observations to narrow bands.

In addition to the requiring high spatial resolution, it is also challenging to separate the light emitted by the planet from that of the star. Imaging techniques such as Angular Differential Imaging (ADI) (**Marois2007**) and Reference Differential Imaging (RDI) (**Lefreniere2009**; **Soummer2012**) provide methods for reducing the stellar point-spread-function (PSF). Coronagraphs are optical elements which suppress the stellar PSF through self-destructive interference or physical occultation, depending on the position in the optical path. The difference in spectra between the planet and the star can also be used to separate the two sources.

Presently, 10m class telescopes such as the Very Large Telescope (VLT) in Paranal, Chile or the Gemini Observatory split between Hawaii and Chile provide the best combination of resolution and instrumentation to perform direct imaging of exoplanets. The NACO instrument at the VLT provided the first image of an exoplanet in 2004 (Chauvin et al., 2004). These observatories are among those equipped with an adaptive optics system, coronographic instrumentation and near to mid infrared imaging and spectroscopic capabilities to directly image exoplanets, with several exemplar systems becoming standard objects of interest. While it's terribly interesting to explore the details of each of these objects, we will focus our discussion on objects will be used further in this study, due to their scheduled observation as part of the JWST GTO and Early Release Science (ERS) programs (Charles A Beichman et al., 2019c). The parameters of these and other directly imaged exoplanets and brown dwarfs are summarized in table 1. (**Lagage2015**)

VHS 1256 b

Originally discovered in 2015 (Gauza et al., 2015a) as part of the VISTA Hemisphere Survey, VHS-1256b is a late-L dwarf in a 102 AU orbit around an M dwarf. (Gauza et al., 2015a) present astrometric, photometric and spectroscopic data on the planet, finding an age of 150-300 Myr from a moving group association, a luminosity $\log(L_{bol}/L_{\odot})$ of -5.05$\pm$0.22 and infer a mass of $11.2^{+9.2}_{-1.8}$ M_{Jup}. The effective temperature is found to be 880^{+140}_{-110} K from evolutionary models. This is substantially colder than field dwarfs of a similar spectral type (typically 1400K), and so it is proposed that a thick Fe and Mg-Si cloud layer acts to reduce the effective temperature. Similar findings are presented by (Rich et al., 2016) using Subaru/IRCS.

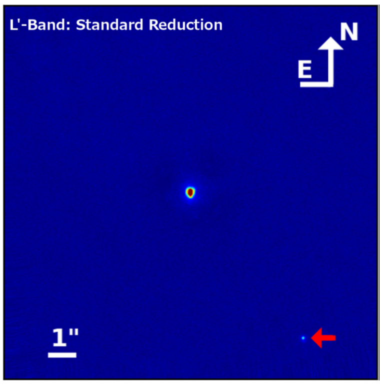

Figure 2: VHS-1256b as observed with Subaru/IRCS in the L'-band (Rich et al., 2016), reduced using the LOCI algorithm (**Galicher2011**).

In (Miles et al., 2018), methane is detected using KECK/NIRSPEC in the L-band. The shallow depth of the feature indicates chemical disequilibrium in the photosphere, as the derived abundance departs from an equilibrium abundance by a factor of 10-100. However, the best fit model retrieves substantially different parameters for temperature (1240 K) when compared to previously published results.

The wide separation (8") and proximity to Earth make VHS-1256b an ideal target for studying atmospheric properties. It will be observed as part of the JWST ERS Program (**Hinkley2019**), where a medium resolution spectrum (R$\geq$1700) will be measured from 0.6-28 micron. This will enable a more precise measurement of the abundance of methane and other species in the atmosphere, and will allow for investigation of the cloud properties in the mid infrared.

2M1207b

Name	d [pc]	Mass [M_{jup}]	Sep [au]	Sep ["]	Age [Myr]	$\log(L_{bol}/L_{\odot})$	T_{eff} [K]	References
Widely separated companions								
VHS 1256b	12.7 ± 1.0	2 ± 1	102	8.1	$10^3 - 10^4$	-5.05 ± 0.22	880	(Gauza et al., 2015a)
Fomalhaut b	7.704 ± 0.028	≤ 2	119	13	440 ± 40	...	1600 ± 100	
Close in companions								
2M1207b	152.4 ± 1.1	2 ± 1	41	0.8	10 ± 3	-4.68 ± 0.05	1600 ± 100	
51 Eridani b	29.4 ± 0.3	2 ± 1	13	0.45	23 ± 3	-5.06 ± 0.2	700	(Macintosh et al., 2015)
β Pic b	19.3 ± 0.2	2 ± 1	9	0.4	23 ± 3	-3.78 ± 0.03	1600 ± 100	(Quanz et al., 2010)
GJ 504b	17.56 ± 0.08	$3 - 30$	44	2.5	$100 - 6500$	-6.13 ± 0.03	544	(Skemer et al., 2016a)
HD 95086b	90.4 ± 3.3	5 ± 2	56	0.6	17 ± 4	-4.96 ± 0.10	1050	(De Rosa et al., 2016)
HR8799b	39.4 ± 1.0	5 ± 1	68	1.7	40 ± 5	-5.1 ± 0.1	870^{+30}_{-70}	(Marois et al., 2008; Skemer et al., 2012)
HR8799c	39.4 ± 1.0	7 ± 2	38	0.95	40 ± 5	-4.7 ± 0.1	1090^{+10}_{-90}	(Marois et al., 2008; Skemer et al., 2012)
HR8799d	39.4 ± 1.0	7 ± 2	24	0.62	40 ± 5	-4.7 ± 0.2	1090^{+10}_{-90}	(Marois et al., 2008; Skemer et al., 2012)
HR8799e	39.4 ± 1.0	7 ± 2	14	0.38	40 ± 5	-4.7 ± 0.2	1000	(Marois et al., 2008; Skemer et al., 2012)
LkCa 15b	145 ± 15	6 ± 4	20	0.08	2 ± 1	...	...	
PDS 70b	113.43 ± 0.52	7 ± 2	23	0.19	5 ± 1	...	900	(Haffert et al., 2019)
PDS 70c	113.43 ± 0.52	4.4 ± 1	30	0.24	5 ± 1	...	10^4	(Haffert et al., 2019)
Nearby Brown Dwarfs								
WISE 0855	2.2 ± 0.2	$3 - 10$	...	...	$10^3 - 10^4$	-10.5	$225 - 260$	(Luhman, 2014; Tinney et al., 2014)
Luhman 16B	1.998 ± 0.0004	28.6 ± 0.3	...	...	$600 - 800$	-4.68	1201	(Garcia et al., 2017; Sahlmann et al., 2015)

Table 1: Summary of directly imaged planet and brown dwarf parameters based on (Bowler, 2016) and references therein. Luminosity for WISE 0855 is calculated in H band.

1.2 BROWN DWARFS

(**Oliveira**) (Helling et al., 2014)(**Cooper2014**) (Nikku Madhusudhan et al., 2018) (**Burrows2003**) (**Marley2014**) (Manjavacas, 2014) (B. Biller, 2017) (Jacqueline K Faherty et al., 2018) (Morley et al., 2014)

1.2.1 Physics

1.2.2 Observational Properties

T-Type

L-Type

Luhman 16B

Y-Type

WISE 0855-0714

1.3 MOTIVATION

1.3.1 Current Status of Atmospheric Characterization

Both exoplanets and brown dwarfs raise interesting questions, but the real challenge is in gathering and processing the data necessary to answer them. The best methods currently in use involve taking spectroscopic data and inferring atmospheric properties from the spectral features. The light we measure may be thermal emission from the planet, where it is absorbed and scattered as it passes through the planet's atmosphere, or it may be light from the planet's host star which passes through the upper layers of the atmosphere. These provide complementary information about the composition and structure of the atmosphere, probing different altitudes and pressures. While a more complete overview of exoplanet atmospheres is covered in the literature (**Seager2010**; Bozza et al., nodate; Nikku Madhusudhan et al., 2014), we will briefly summarize the current methods used and what has been learned so far.

Transmission Spectroscopy

(Kreidberg, 2018) (Lee et al., 2012) (MacDonald et al., 2017) (**Madhusudhan**)

Emission Spectroscopy

(B. A. Biller et al., 2018) (Danielski et al., 2018) (GRAVITY Collaboration et al., 2020)

1.3.2 JWST Studies

(Charles A Beichman et al., 2019c)

Early Release Science

GTO Programs

1.3.3 Biosignatures and Future Missions

1.4 THESIS OVERVIEW

With sufficient background and motivation, we will now outline the remainder of this thesis.

Chapter 2 will provide a more extensive background of the James Webb Space Telescope, and in particular the MIRI Medium Resolution Spectrometer (MRS). We will outline the principle optical components dedicated to integral field spectroscopy, as well as the detector characteristics of MIRI. This will provide the necessary background to understand the instrumental and optical effects discussed in Chapter 3.

The third chapter examines the fringing effect in the MIRI MRS instrument. We discuss the optical effects that result in fringing patterns, as well as outlining current and future strategies for fringe correction. We describe the creation and processing of our mock observations using the MIRI instrumental simulator and the JWST data reduction pipeline. With the degraded spectra from the simulated data, we measure the impact of fringing on spectral extraction using cross correlation techniques, and and how this impacts molecular mapping studies. This in turn motivates Chapter 4, where the species identified using molecular mapping can justify the inclusion or exclusion of particular species in an atmospheric retrieval.

In Chapter 4 we explore atmospheric retrievals with the MIRI MRS. We outline our procedure for performing a retrieval using the petitRADTRANS radiative transfer code and Multinest as an implementation of the nested sampling strategy for parameter space exploration We measure the impact of fringing on parameter estimation, and also investigate how observing parameters will impact retrievals, discussing the advantages and challenges of studying atmospheres in the mid infrared.

Finally we summarize and discuss our finding and future investigations in the final chapter.

2 MIRI: THE MID-INFRARED INSTRUMENT

MIRI is an instrument that will provide unique capabilities for studying exoplanets and other cold and distant objects. This chapter will provide a detailed overview of the technical details and capabilities of the instrument. A complete description of MIRI is provided in a series of papers from (Boccaletti et al., 2015; Bouchet et al., 2015; Glasse et al., 2015; P. Lagage et al., 2015; Ressler et al., 2015; Rieke et al., 2015b,c; Wells et al., 2015; Wright et al., 2015).

2.1 THE JAMES WEBB SPACE TELESCOPE

JWST is a 6.5m space based observatory built in collaboration between NASA, ESA and CSA that will be located in a halo orbit at the L2 Earth-Sun Lagrange point. As the successor to the Hubble Space Telescope and the Spitzer Space Telescope, it will provide a new perspective for infrared astronomy. It is currently scheduled to launch in March 2021.

James Webb is fully optimized for infrared astronomy. To reduce instrumental thermal background, the entire telescope will operate at cryogenic temperatures. A large sun-shield will help block solar infrared radiation. The lightweight beryllium mirrors are coated in gold to maximize reflectivity out to the mid infrared.

Of key interest to exoplanet science is the both the sensitivity and spatial resolution of the instrument. With its 6.5m primary, JWST will have a spatial resolution from 0.01" at 0.6 micron to 0.92" at 29 micron. The increase in sensitivity is due in part to the larger collecting area, but also to advances in detector technology since the previous generation of infrared observatories. For example, the MIRI instrument will have a minimum detectable flux of 0.13 μJy at 5.6 micron, or roughly a factor of 1000 better than what was possible with the Spitzer Space Telescope (Glasse et al., 2015).

There are four primary instruments that constitute the Integrated Science Instrument Module (ISIM). Near-Infrared Camera (NIRCam), which provides imaging with coronagraphic capabilities from 0.6-5 micron. The Near-Infrared Spectrograph (NIRSpec) provides fixed slit and integrated field unit spectroscopy capable of analyzing multiple objects simultaneously, and operates in the same wavelength range as NIRCam. The Fine Guidance Sensor/ Near-Infrared Imager and Slitless Spectrograph (FGS/NIRISS) allows for low and medium resolution spectroscopy with high photometric stability, as well as aperture masking interferometry. The final instrument, MIRI, is the subject of this thesis.

Figure 3: The James Webb Space Telescope during integration of the telescope into the Spacecraft Element (**assembled**).

Subsystem
Imaging
4QPM Coronagraphic Imaging
Lyot Coronagraphic Imaging
Low Resolution Spectroscopy
Medium Resolution Spectroscopy

Table 2: Summary of MIRI observing modes.

2.2 MIRI

The Mid-Infrared Instrument (MIRI) provides imaging, fixed slit and integrated field spectroscopy between 4.8 and 28 micron (**Rieke2015**). It will operate at a temperature of 6.7K to reduce instrumental backgrounds over its wavelength range of 0.6-28.8 micron.

(**Kendrew2015**)

2.3 THE MEDIUM RESOLUTION SPECTROGRAPH

The Medium Resolution Spectrograph (MRS) consists of four integrated field spectrographs projected onto two detectors, covering 4.8-28 micron with a spectral resolution varying from R=1700 to R=3500.

(**Wells2015**)

Channel	Sub-band	Band	Detector	λ Range [μm]	FOV [as]	$\lambda/\Delta\lambda$
1	Short	1A	SW	4.83 - 5.82	3.46×3.72	3500
	Medium	1B		5.62 - 6.73	3.46×3.72	3500
	Long	1C		6.46 - 7.76	3.41×3.72	3300
2	Short	2A	SW	7.44 - 8.90	4.16×4.76	3000
	Medium	2B		8.61 - 10.28	4.16×4.76	3000
	Long	2C		9.94 - 11.87	4.12×4.76	3000
3	Short	3A	LW	11.47 - 13.67	6.00×6.24	2700
	Medium	3B		13.25 - 15.80	5.96×6.24	2300
	Long	3C		15.30 - 18.24	5.91×6.24	2300
4	Short	3A	LW	17.54 - 21.10	7.14×7.87	1700
	Medium	3B		20.44 - 24.72	7.06×7.06	1700
	Long	3C		23.84 - 28.82	6.99×7.87	1500

Table 3: Properties of the MIRI MRS channels (Wells et al., 2015).

2.3.1 Coordinates

There are three primary coordinate systems in use with JWST/MIRI-MRS, of which two will be relevant for this thesis, with the detector and local MRS coordinates described in Fig. 4 (Argyriou et al., nodate).

The detector coordinate grid is formed by counting x/y pixels, as well as the slice number. Each of the two MRS detectors is an array of 1032×1024 pixels, though only 1024 are photosensitive in the horizontal direction. Each image slice from the IFU appears as a curved stripe on the detector, though neighboring stripes on the detector do not correspond to neighbouring slices of the image.

The local MRS coordinate system is described in terms of α, β and λ. The continuous α coordinate is the along slice direction, while *beta* is perpendicular and discrete, corresponding to the slice number. λ is the wavelength. Both α and λ are fit by a second order polynomial to account for along and across slice distortion (Wells et al., 2015). Each detector sub array has its own mapping to α, β, λ space, due to the differences in FoV, slice count, distortion and spectral resolution.

The third coordinate frame is the global coordinate system of JWST itself, V1,V2,V3. The V1 coordinate refers to the symmetry axis of the telescope, V3 points towards the foldable secondary mirror support structure strut. V2 completes the coordinate system, being orthogonal to V1 and V3. This coordinate system will not be used in this thesis.

2.3.2 Integrated Field Spectroscopy

2.3.3 Optical Systems

Channels, bands, etc **ref:Chen2019**

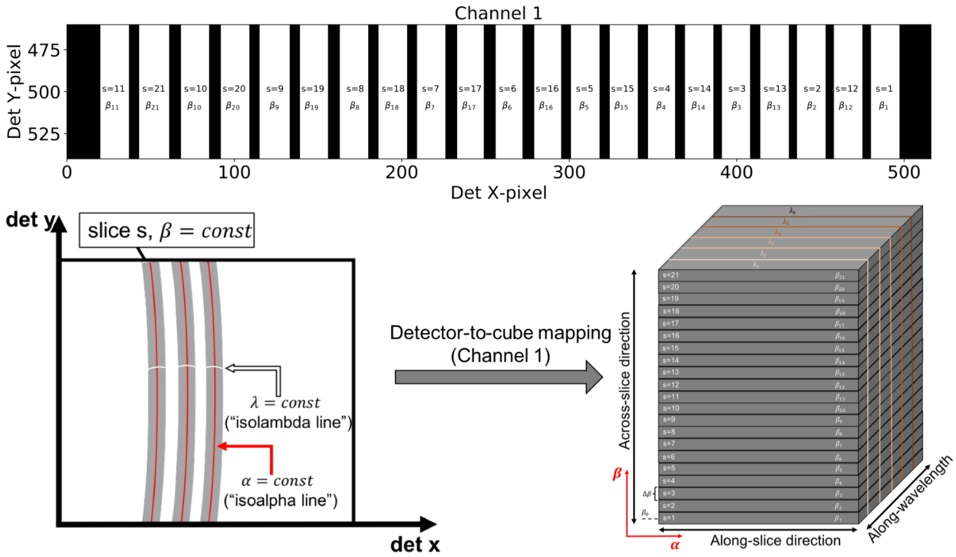

Figure 4: Description of the MRS detector (x,y,s) coordinate system to the local MRS (α, β, λ) cube coordinates. **Top**: Detector coordinates. Note that the consecutive stripe numbers s_i, s_{i+1} correspond to neighbouring image slices. **Bottom**: Description of the (invertible) detector-to-cube transformation (Argyriou et al., nodate).

Figure 5: Detector images of a spatially and spectrally flat calibration source for the SW detector (left) and LW detector (right).

2.3.4 Detectors

Readout Modes

2.4 OBSERVATIONS

2.4.1 Dithering

2.4.2 Exposure time calculations

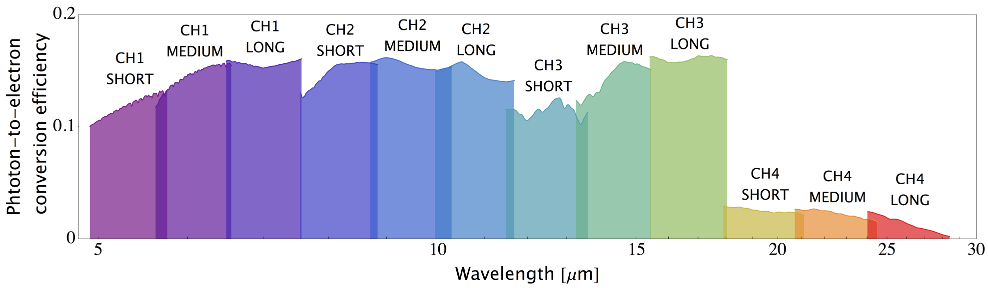

Figure 6: Average photon-to-electron conversion efficiencies for the MIRI MRS detectors

3 FRINGING EFFECTS IN MIRI

Understanding optical and instrumental effects is critical for creating accurate simulated observations and for characterizing systematics. These systematics and uncertainties in turn impact the potential science results from any instrument by biasing measurements, reducing the signal to noise ratio of measurements or by injecting non-physical signals and correlations. The aim of this chapter is to examine fringing in the MIRI detectors and how this effect is modeled in the instrumental simulator (MIRISIM). We will examine the current status of fringe modeling and correction before discussing the modifications made to the MIRI instrumental simulator in order to model point-source fringing effects.

In order to quantify the effect of fringing on a spectrum, we examine the effect of fringing on a cross correlation between the extracted spectrum from the instrument and a known template. This provides a measure of the extent to which the signal has been degraded. In addition we examine the impact of this on the science case of molecular mapping, where cross correlations between a cube of IFU data and a molecular spectral template are used to identify the presence of a given species in an observed object.

3.1 FRINGING

Thin film interference occurs when light is coherently reflected at the boundary between two layers and interferes with the incident light. This is the principle on which Fabry-Pérot interferometers function. As we wish to determine the effect of fringing on the amplitude of the signal received by the detector as a function of wavelength, we are effectively interested in the transmittance of a series of Fabry–Pérot interferometers. Assuming an ideal plane-parallel optical cavity with a reflectance R at both boundaries, thickness D, and an angle θ at which the light travels within the cavity, we can compute the transmittance as:

$$T_c = \frac{1}{1 + \frac{4R}{(1-R)^2}\sin^2\left(\frac{\delta}{2}\right)} \tag{1}$$

Where the phase δ at half a wavelength ($\phi = \pi$), with wavenumber σ is:

$$\delta = 4\pi\sigma D\cos\theta - (\phi - \pi) \tag{2}$$

Systems with a spacing on the order of micrometers to millimeters produces significant interference for infrared light (Lahuis et al., 2003).

The detectors of the MRS consist of several layers, as shown in Fig. 7, with a characteristic thickness of tens of micron, which results in significant (10%-30%) 'fringing' in a spectrally flat signal - visible in Fig. 5. The geometric thicknesses of the detector layers are given in table 4.

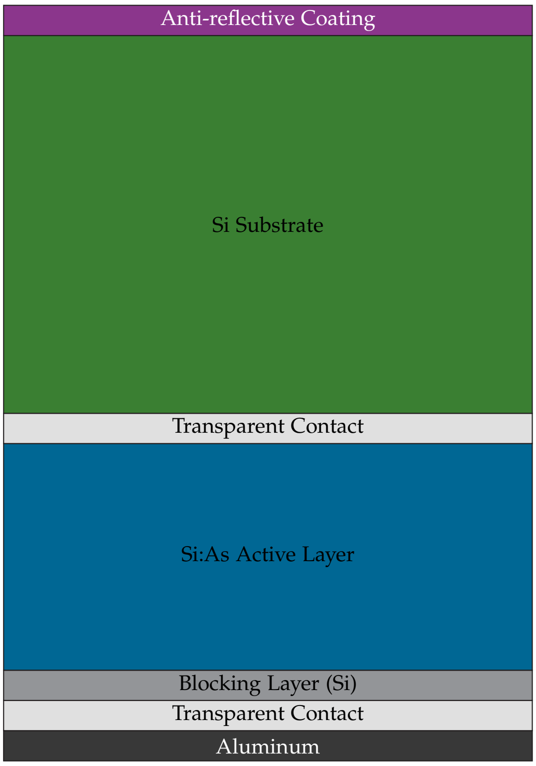

Figure 7: Layers of the MIRI MRS detectors. Note that thicknesses are not to scale (Rieke et al., 2015c).

While this is typical for infrared detectors such as those in the Spitzer Space Telescope (Lahuis et al., 2003) or in the Space Telescope Imaging Spectrograph on board HST (**Malumuth2003**), the sensitivity and spectral resolution of the MRS increase the significance of this issue. The MIRI consortium has stated that the error budget for all detector effects must be 3.3% or less. Present fringing corrections result in a 5% deviation from a photometrically accurate signal, and can introduce correlated noise which will degrade any measured spectrum. Therefore it is critical to examine the impact of fringing on a signal, the parameters that influence the fringing strength and phase, and possible solutions for fringe correction. If all of the geometric and optical parameters were known, this would be sufficient to numerically solve for the fringing pattern within MIRI using eqn 1. Unfortunately, uncertainties in the thickness in the detector layers, variations in the layer deposition thickness, and the uncertainty of transmittance and reflectance of the materials used at cryogenic temperatures prevents the implementation of such a numerical model. Instead, we will turn to calibration data taken to empirically characterize the fringing pattern.

While a more complete treatment of proposed fringe correction can be found in (**Argryiou2020**) and (Fred Lahuis et al., 2018), this work will examine the implementation of fringing into the MIRI instrumental simulator and address the current state of fringe correction in the JWST Data Calibration Pipeline. We will discuss the architecture and usage of MIRISIM, along with the modifications we have made in order to model point-source fringing.

Layer	Material	Depth [μm]	Comments
Anti-Reflection Coating	ZnS	0.66	Optimized for $\lambda = 6\mu$m.
Substrate (raw wafer)	Si	460	Inactive layer.
Bottom Transparent contact	?	?	Not transparent, negative applied bias voltage.
Active layer	Si:As	35	Photoelectric absorption layer.
Blocking layer	Si	4	Inactive layer.
Top transparent contact	?	?	Not transparent. Positive applied bias voltage.
Pixel metalization	Al	semi-infinite	Forms metallized electrical contact with top transparent layer.

Table 4: Detector layer compositions and geometric thicknesses.

3.1.1 Current Status of Fringing Correction

Three test campaigns have been run in order to characterize MIRI: the Flight Model (FM) in 2008-09, the Cryogenic Vacuum (CV) in 2015-16, and the Optical Telescope element/ Integrated Science (OTIS) tests in 2017. Fringing was a major subject of both the FM and CV campaigns The first fringe model is fit to a spectrally flat, spatially extended source based on the FM test data. This is used to derive a 'fringe flat', and example of which is presented in 8.

However, due to the dependance of fringing on the incident angle of the light, a single model of fringing is insufficient to describe the full effect. Therefore, we use data taken in XXXXXXXXXX at various points across the detector and quantify how this changes the extracted spectra after processing in the JWST pipeline.

DESCRIBE HOW THE DATA WAS TAKEN HERE. - Problems with point vs extended sources - multiple collection runs (VanderPlas, 2018)

Fred Lahuis et al., 2018

3.2 MIRISIM

Consortium2018 Cossou2019 The MIRI instrument has been modeled in python as a program known as MIRISM. This program takes in an astronomical 'scene' along with some configuration parameters to output a detector data product, similar to what will be produced by the actual instrument. MIRISIM is relatively full-featured simulator, modeling the instrumental PSF, various noise sources and distortion maps, among other effects. While MIRISIM is functional for all of the MIRI sub-instruments, this report will only deal with the Medium-Resolution Spectrometer (MRS) sub instrument, described in section 2.3. The objective of this section is to describe the implementation and testing of an updated optical model of the 'fringing' effect - an optical effect caused by thin film interference from the multiple layers of the detector.

Figure 8

3.2.1 Architecture

SCENE - SEDs SIMULATOR PYSPECSIM

3.2.2 Data Products

3.2.3 Fringing Model Implementation

Ultimately this data collection produced a series of 'fringe-flats' of an almost point like at various position across the detector and in each channel. We implemented a new routine into the pySpecSim portion of MIRISIM to read in the location of point sources within a scene, and apply the correct position dependent fringe flat. This implementation comes with several caveats: namely that the fringing model is not yet fully developed, so it can only be considered accurate for point sources located at the same (α, β) location as the source used to produce the fringe flat. Additionally, the source used to generate the data is not a true point source, nor are there fringe flats produced for the full MRS wavelength range. We stress that the goal of this testing is to demonstrate the significance of this effect to justify the need for a more complete model along with additional calibration data to constrain the detector layer parameters.

3.3 JWST PIPELINE

Bushouse et al., 2015 **Labiano-Ortega2016**

3.3.1 Stage 1 Processing

The raw data files read from MIRISIM (or eventually the MIRI instrument itself) are a series of *exposures*, each made up of set of *integrations* containing a some number of *groups* or frames. Each group is a non-destructive readout of the detector arrays, providing a series of increasing counts known as ramps in DN/s (digital number per second). The first stage of the JWST pipeline takes these raw files, applies a series of steps and outputs a single file for each input exposure in units of countrate. This procedure is applied to any MIRI data. We used default pipeline settings to apply this procedure, and applied all steps applicable to the MIRI instrument.

3.3.2 Stage 2 Processing

For the second stage of processing we use the Stage 2 Spectroscopic Processing pipeline, and apply the steps individually to maintain control over parameters. The second stage pipeline applies instrument specific corrections that result in a photometrically calibrated exposure. For the MRS, this involves the following series of steps, some of which will be described in further detail below.

1. `assign_wcs` Assign a World Coordinate System (WCS) to each exposure.
2. `flat_field` Flatten photometric variation from differences in gain and dark current.
3. `srctype` Assign whether the target is a point or extended source based on input from the raw data files or observation parameters.
4. `straylight` Remove known stray light component.
5. `fringe` Divide by an extended source fringe flat.
6. `photom` Photometrically calibrate the exposure based on known pixel sensitivities and areas.
7. `cube_build` Transform from a (set of) 2D detector images to a 3D IFU cube in (α, β, λ).

Photometric Calibration

Photometric calibration is the process of removing detector and optical biases to ensure that the measured output corresponds to the true flux incident onto the telescope. This process occurs in the PHOTOM step of the JWST pipeline, and uses reference files which store per-pixel photon-to-electron conversion efficiencies to transform the count rate data product to a flux measurement. This corrects for the wavelength dependent bias shown in Fig. 6.

However, this step remains under development, and does not produce absolutely calibrated images. In particular, even using the most up to date reference files (v8D.04.00) there remains discontinuities between channels, and poorly calibrated slopes.

Fringing correction

Carnall, 2017

Cube Building

Aperture Photometry

Once the data from the pipeline has been transformed into a spectral cube, we can perform aperture photometry using the `photutils` package to extract a 1D spectrum of the source. For each frame in each sub-band the coordinates of the spaxel at with the peak flux is detected using `photutils find_peaks`, which provides the location for the center of a circular aperture. A radius of 5 spaxels is used to encompass the entire PSF for a point source. If the files have already been photometrically calibrated, measuring the flux requires just adding the flux from each spaxel within the defined radius for each frame. While optimal extraction techniques exist, given our known input signal and background, this procedure is adequate for producing a spectrum in each sub-band, which can then be combined into a single spectrum for all measured sub-band.

Unfortunately, due to the issues described above with the PHOTOM step of the JWST pipeline, the spectrum built using aperture photometry does not accurately reflect the input spectrum in slope or absolute photometry. Therefore, we correct the extracted spectrum channel by channel. We fit a cubic polynomial to a median filtered copy of both the template spectrum and the extracted spectra. The cubic fit to the extracted spectra is subtracted from the data, and the fit to the template is added. Thus this procedure corrects the slope and median flux value, but does not affect high frequency noise or signals. Fig. 9 shows an example of the results of this procedure. We believe that this is a justified measure, as the errors with photometric calibration in the pipeline should be resolved before first light of the telescope.

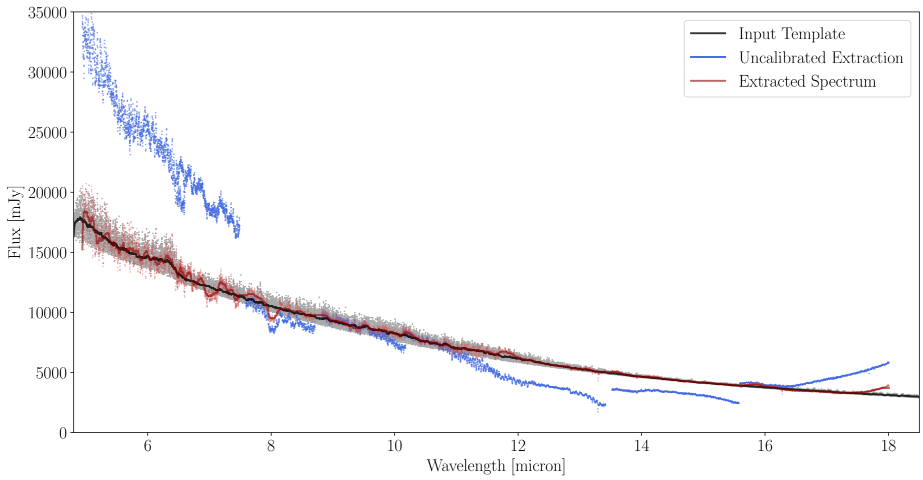

Figure 9: Comparison of an input spectrum generated using petitRadTrans and the empirically calibrated output spectrum after extraction from the cube produced by the JWST pipeline.

3.3.3 Cross-Correlation

Ignas Snellen et al., 2014Simkin, 1974 **Tonry1979** Petermann, 2019 Bodis, 2007 To quantify the similarity of the spectrum output by the JWST pipeline to the input into MIRISIM, we rely on the technique of cross correlation. For two arbitrary, complex-valued functions $f(t)$ and $g(t)$, we can compute the cross correlation as as function of the shift τ between the functions (typically in time or velocity space):

$$(f \star g)(\tau) \equiv \int_{-\infty}^{\infty} f^*(t) g(t+\tau) dt \tag{3}$$

Our signals of interest are astrophysical spectra, measured in a finite number of discrete wavelength bins. For such a signal with M bins:

$$(f \star g)[n] \equiv \sum_{m=0}^{M} f^*[m] g[m+n] \tag{4}$$

Care must be taken when cross-correlating signals, as differences in normalization can result in changes in the correlation coefficient. Our procedure takes in two spectra. The first is an emission spectrum produced by the petitRadTrans program P. Mollière et al., 2019, which provides our forward model with which we compare our data spectrum. Our data is the result of passing the template spectrum through MIRISIM, and extracting it from the resulting detector image using the JWST pipeline. We then rebin the high-resolution input spectrum to the same wavelength bins as the data spectrum, using the `spectres` package. Prior to normalization, we remove any outliers from the spectrum (due to binning errors or instrumental effects) by setting any data points separater by more than 15 standard deviations from the mean to the median value of the spectrum. For each spectrum, we subtract the minimum value to remove any offset in the spectrum, and divide by the maximum value to restrict the range to [0,1]. We then use apply a Savitzky-Golay filter with a window of 1/4 the length of the spectrum and a polynomial order of 3, which we then subtract from the unfiltered spectrum. This removes the continuum emission from the spectrum, and centers it around 0. We then renormalize the spectrum by dividing by the maximum absolute value such that the range is in [-1,1]. The cross correlation between the forward model and itself is computed, excluding the region of interest around 0 offset. This 'autocorrelation' is subtracted from the cross correlation between the forward model and the data spectrum in order to remove secondary peaks. Finally, we normalize the cross correlation by the standard deviation of the cross correlation (excluding the central peak), giving an output measured as a signal to noise ratio.

3.4 RESULTS

		MIRISIM Fringing Model			
		None	FM Extended	FM Point On Axis	FM Point Off Axis
Correction	None				
	Ext. Flat				

Figure 10: Normalised Input/Output Spectrum for VHS-1256b, Residuals, Hists, Cross Corr

3.4.1 Residual Statistics

In addition to computing the cross correlation between the forward model and the data spectrum, we also examine the residuals between the two spectra. Here we can see any unexpected variations between the two (periodic signals, offsets or other features). We can also examine a histogram of the residuals, normalized by the standard deviation of the data spectrum. This provides us with a distribution which should have a mean of 0 and unit width if the data are unbiased and share a distribution with the true input spectrum.

3.4.2 Fringing Results

1. A stronger input signal results in a stronger correlation. 2. Fringing does NOT necessarily degrade the cross correlation SNR, but rather increases it. The scale of this increase seems to depend on the absolute magnitude of the correlation (ie, a larger increase at higher SNR) 3. The residuals from subtracting the template from the data has structure. 4. If the residuals are histogrammed (and normalized by the standard deviation of the data), the width of the distribution may correspond to the cross correlation SNR (wider distribution = lower SNR) 5. Only when strongly increasing the fringing effect does the SNR decrease. 6. Correcting for fringing using the standard JWST fringe map decreases the SNR when compared to the case of fringing with no correction, but is typically still above the no-fringing case. 7. The JWST correction performs worse in the off axis case, as the fringe pattern begins to vary more when compared to the CV fringing model.

3.4.3 Molecular Mapping

4 ATMOSPHERIC RETRIVALS

Everything photon of light that we receive from an exoplanet will interact with its atmosphere, and will therefore provide us with a hint of what that atmosphere may look like. An atmospheric retrieval is the process of reconstructing the atmosphere of an object based on an observed spectrum. This process relies heavily on having accurate models which can be parameterized by the physical quantities we are interested in: generally the temperature, pressure and composition (Nikku Madhusudhan, 2018). As these models cover a very large parameter space (>10 parameters, each covering several orders of magnitude), it is necessary to have an efficient method for sampling this space, computing a model and comparing this model to the data (Bjoern Benneke et al., 2012).

This chapter will outline the process of an atmospheric retrieval from modelling to marginalization of posteriors, and will examine the impact that the instrumental effects described in chapter 3 have on the retrieved parameters. Additionally, this will provide an example of how the MIRI MRS can be used to explore exoplanet and brown dwarf atmospheres, and what observational parameters should be considered when studying these objects.

Schlawin et al., 2018 Fisher et al., 2019 **Oreshenko2019**Barman et al., 2015 Björn Benneke, 2013 Bjoern Benneke et al., 2012 **Blanco-Cuaresma2018** Konopacky et al., 2013

(Morley et al., 2018) Lupu et al., 2016 Gandhi et al., 2018 Baudino et al., 2017 Line et al., 2013 **Madhusudhan2018b** Irwin et al., 2008 Robinson et al., 2016 Waldmann et al., 2015b Waldmann et al., 2015a Line et al., 2015, 2017; Zalesky et al., 2019

Batalha et al., 2018Feng et al., 2018 P. Mollière et al., 2019

Atmospheric Modeling

Atmospheric modelling is the task of creating an spectra based on the physical properties of the atmosphere. This is a broad task that can range from a 3D Global Circulation Model (GCM) which accounts for self-consistent atmospheric chemistry (Chen et al., 2019) to a 1D model based around an empirical temperature-pressure profile (P. Mollière et al., 2019). The choice of model depends largely on the requirements for accuracy and computational cost. Considering the potentially millions of possible atmospheres that must be examined in a retrieval problem, whatever model is used must be computationally efficient above all else.

4.1 PETITRADTRANS

For this work we chose to use the petitRADTRANS package due to its user-friendly python implementation, high speed computation for retrieval

Property	Description
Temperature	Parameterized, e.g. (Guillot, 2010)
Abundances	Parameterized, e.g. vertically constant
Scattering	Cloud scattering, transmission spectra only
Clouds	Power law and condensation clouds
Cloud particle size	f_{SED} and K_{ZZ} or parameterized
Particle size distribution	log-normal, variable width
Cloud abundance	Parameterized
Wavelength spacing	R=1000 (c-k), 10^6 (lbl)
Valid emission spectra	Clear, from NIR and longer

Table 5: Description of the parameters available in petitRADTRANS. For cloud particles, f_{SED} is the mass-averaged ratio of the cloud particle settling speed and mixing velocity. K_{ZZ} is the atmospheric eddy diffusion coefficient (Ackerman et al., 2001)

use and extensive high resolution, line-by-line spectral library for generating planetary spectra (P. Mollière et al., 2019). It is a 1D, radiative transfer package with many parameters options, described in table 5 PetitRADTRANS can compute both emission and transmission spectra, with an output spectral resolution of R=1000 in correlated k mode, or R=1 000 000 in line-by-line mode.

Note that much of the following sections applies to many other similar 1D radiative transfer atmospheric modelling programs such as ATMO (**Goyal2018**), Planetary Spectrum Generator (**Villanueva2018**), HELIOS (Malik et al., 2017, 2019) and others. Many (or even most) of these programs rely on the same set of high-resolution molecular line lists, including HITRAN/HITEMP (**Rothman1973**; Gordon et al., 2017; Rothman et al., 2010), ExoMol/ExoCross (**Tennyson2016a**; Tennyson et al., 2016; Yurchenko et al., 2018) and others.

4.1.1 Radiative Transfer

In order to compute the emission spectrum an initial featureless blackbody spectrum $B(T_{int})$ is passed through multiple discrete layers of the atmosphere, parameterized by their temperature, pressure, and the opacities of each of the species present in a given layer. Modeling each layer as plane parallel, the intensity is computed as in (Irwin et al., 2008; P. Mollière et al., 2017, 2019)

$$I_{top} = B(T_{int})\mathcal{T}^{atmo} + \frac{1}{2}\sum_{i=0}^{N_L-1}\left[B(T^i) + B(T^{i+1})\right]\left(\mathcal{T}^i - \mathcal{T}^{i+1}\right) \tag{5}$$

N_L is the number of layers in the atmosphere, and $\mathcal{T}$ is the transmission from a given layer to the top of the atmosphere. All quantities are averaged per wavelength bin in c-k mode, while they are evaluated at each wavelength point in line-by-line mode.

(Guillot, 2010)

4.1.2 Opacity Sources

To compute the emission spectra of an atmosphere, petitRADTRANS accounts for various opacity contributions including absorption and emission lines, collisionally induced absorption, cloud opacity and scattering and Rayleigh scattering cross sections. These sources are described in detail in (P. Mollière et al., 2019), summarized in tables 2 and 3. For this work we consider only the case of a cloud-free atmosphere due to the complexity of realistic cloud modeling.

Line-by-line

In its high resolution line-by-line mode, petitRADTRANS computes emission spectra with R=10^6. These spectra are computed using opacity sources for molecular and atomic lines from ExoMol/ExoCross library (Yurchenko et al., 2018). Pressure broadening is taken into account using the coefficients from HITRAN/HITEMP (Rothman et al., 2010, 2013) or from (**Sharp2007**) (Eqn. 15). The line opacities are computed from 80-3000K, and from 0.3-28μm in high resolution mode.

Correlated K

The low resolution mode of petitRADTRANS uses the correlated-k (c-k) method of computing line opacities (Fu et al., 1992; Goody et al., 1989; Lacis et al., 1991). This method for calculating emission and absorption features assumes that the opacity distribution functions between differing species are uncorrelated, which permits simple computation of overlapping features. While petitRADTRANS implements a c-k method with a spectral resolution of 1000, in principle it is accurate to much higher resolutions. However, the principle utility of the c-k method is in the dramatic reduction in computational cost for computing a spectra such that petitRADTRANS can be used as the foundation for an atmospheric retrieval code requiring hundreds of thousands or millions of models to be generated. (P. Mollière et al., 2019) discusses the variations between the results of the line-by-line method and the c-k method, finding discrepancy of at most 6%. Typical variation is much lower, as seen in Fig. 2 of (P. Mollière et al., 2019).

Clouds

Line et al., 2016 Jacqueline K Faherty et al., 2018 Morley et al., 2014 Lavie et al., 2017

4.2 BAYESIAN INFERENCE

An atmospheric retrieval is the process of extracting information about physical parameters from a measured spectrum. In general this procedure involves comparing the data to a series of template spectra with known parameters and identifying the best fit model. Unfortunately for astronomers, atmospheres are complicated: typical one 1D models still require many (>15) parameters to generate a somewhat realistic model. This results in a very large parameter space in which to search for the correct set of properties that describe our measurement.

Monte Carlo methods, including Nested Sampling, are used to effectively search this large space using the Baysian evidence as a goodness-of-fit metric. Here we will follow (Joshua S. Speagle, 2019) to provide a brief overview of Bayesian inference.

To measure the likelihood of a given model, we turn to Bayes' Theorem:

$$P(\mathbf{\Theta}_M|\mathbf{D}, M) = \frac{P(\mathbf{D}|\mathbf{\Theta}, M)P(\mathbf{\Theta}|M)}{P(\mathbf{D}|M)} \tag{6}$$

In our notation, $\mathbf{\Theta}$ is the set of parameters that describe a model M, that is fit to the data $\mathbf{D}$. Bayes' theorem asks what is the probability that the parameters $\mathbf{\Theta}$ are true given the data and model. The distributions for each parameter are the **posterior** distributions.

This is then related to the **likelihood** $P(\mathbf{D}|\mathbf{\Theta}, M)$ of measuring the data given the model, the **prior** probability $P(\mathbf{\Theta}|M)$ which describes our degree of belief in our model and the **evidence** $P(\mathbf{D}|M)$, which is marginalized over all possible $\mathbf{\Theta}$ and quantifies how well the model describes the data. To simplify notation, we adopt the following convention for Bayes' theorem:

$$\mathcal{P}(\mathbf{\Theta}) = \frac{\mathcal{L}(\mathbf{\Theta})\pi(\mathbf{\Theta})}{\mathcal{Z}} \tag{7}$$

In general, the goal of an atmospheric retrieval is to find the best fit model by maximizing the evidence $\mathcal{Z}$, and as a by product finding the marginalized posterior distributions for each parameter. This comes with many challenges, especially when dealing with large numbers of parameters. Selection of the priors and model will determine the extent to which a result can be interpreted, while sampling large parameter spaces and computing likelihoods introduces substantial numerical challenges. The Markov Chain Monte Carlo method and the Nested Sampling method described below attempt to solve the challenges of exploring a large parameter space.

4.2.1 MCMC

Foreman-Mackey et al., 2013 MacKay, 2003

4.2.2 Nested Sampling

Nested sampling attempts to address several of the shortcomings of MCMC methods while simultaneously improving computational efficiency (Skilling, 2004). MCMC methods generate samples 'proportional to' the true posterior distributions, which lead to difficulties in computing the evidence $\mathcal{Z}$ (Joshua S Speagle, 2020). In contrast, nested sampling puts the evidence first and provides estimates of the posterior distributions from the importance weights of the final set of samples. First described in (Skilling, 2004), nested sampling has been adopted as the sampling algorithm of choice within the astrophysics community (Buchner et al., 2014; F. Feroz et al., 2009; Farhan Feroz et al., 2019; Joshua S Speagle, 2020).

With the goal of parameter estimation, nested sampling attempts to estimate the evidence $\mathcal{Z}$ rather than directly sampling the posteriors (Skilling, 2004). This is done by integrating over the entire parameter space of $\mathbf{\Theta}$

$$\mathcal{Z} = \int_{\Omega_{\mathbf{\Theta}}} \mathcal{L}(\mathbf{\Theta})\pi(\mathbf{\Theta})d\mathbf{\Theta} \tag{8}$$

This is difficult.

Rather than attempting to directly solve the entire multidimensional integral, nested sampling transforms this into an integration over the *prior* volume X:

$$\mathcal{Z} = \int_{\Omega_{\mathbf{\Theta}}} \mathcal{L}(\mathbf{\Theta})\pi(\mathbf{\Theta})d\mathbf{\Theta} = \int_0^1 \mathcal{L}(X)dX \tag{9}$$

This is now a contour integral over isocontours $\mathcal{L}(X)$ which bound the prior volume

$$X(\lambda) = \int_{\Omega_{\mathbf{\Theta}}:\mathcal{L}(\mathbf{\Theta})\geq\lambda} \pi(\mathbf{\Theta})d\mathbf{\Theta} \tag{10}$$

which is the fraction of the prior where the likelihood of the data given the model is above some threshold λ. The integration is now simplified into a 1D integration over X, given proper prior selection.

Method

Consider a parameter space with D dimensions. We will describe this space as a unit hypercube, where each parameter runs from 0 to 1. Priors are thus transformations from this space to a physical parameter space. Often the prior is a uniform distribution, which simply scales the space, but it may also be an informative prior such as a normal distribution centered at an expected physical value. In order to sample this space, N_L 'live points' are generated, each of which provides a set of parameters $\mathbf{\Theta}$. N_L must be greater than $D+1$, and typically values on the order of $50 \times D$ are used (F. Feroz et al., 2009). Using a likelihood function $\mathcal{L}(\mathbf{\Theta})$, the evidence $\mathcal{Z}$ can be computed by comparing the model to the data. Having computed the evidence at each point, the live points are then sorted and the point with the lowest evidence is discarded. A set of ellipsoids is drawn around the remaining points. The procedure for computing these ellipsoids is given in (F. Feroz et al., 2008, 2009). By using a set of ellipsoids, multiple modes in the parameter space can be encompassed. Once the ellipsoids bounding the remaining points are drawn, a new sample is drawn from within the restricted sample space. The evidence for the new point is computed, and it is accepted if the evidence is greater than the minimum evidence of the previous remaining set of points. The entire procedure is repeated until some convergence criteria is satisfied, with each iteration resulting in a smaller volume being encompassed by the ellipsoids, nested within the previous volume.

This procedure can be improved in many ways, including importance nested sampling (Farhan Feroz et al., 2019) and dyamic nested sampling (Joshua S Speagle, 2020).

4.2.3 Multinest

For our implementation of an atmospheric retrieval code, we chose to use the Multinest algorithm (F. Feroz et al., 2009) using the pyMultinest wrapper (Buchner et al., 2014) and using importance nested sampling to improve the accuracy of the Bayesian evidence calculation (Farhan Feroz et al., 2019). This particular implementation of nested sampling is commonly used in atmospheric retrieval codes due to its fast Fortran implementation, though it was initially developed for cosmological problems.

Using the pyMultinest package, we implemented the required log-prior function which transforms the unit hypercube to physical parameter space and the log-likelihood function used to compare the model to the data. The full code is available at `https://github.com/nenasedk/petitRetrieval`, and is based of the emission spectrum retrieval described in (P. Mollière et al., 2019). Retrievals were typically performed using 500 or 1000 live points, with the convergence criteria

$$\Delta \ln \mathcal{Z} = \ln Z_i - Z_{i+1} \tag{11}$$

set to 0.3 for parameter estimation and 0.8 for model comparison, as suggested in the pyMultinest documentation.

4.3 OBSERVATIONS

The targets used in our retrieval study ar guided by the JWST ERS and GTO programs. This allows us to use well-defined observing strategies for each object, and present a clear case for the science that can be accomplished with these observations. While all three were discussed in Chapter 1, we will now outline the proposed observing strategies and science cases for each target.

VHS-1256B

VHS-1256b is a young (0.2Gyr), high mass (11.2M_{Jup}) planet at a distance of 12.7pc (Bowler, 2016). The wide separation of 8" makes it an easy target for observation with the MRS, as its host star will fall outside of the FoV. It has a J-band magnitude of 16.662, and a late L spectral type (Miles et al., 2018). As an object of interest for the JWST ERS program 1386, it will be observed with the NIRCam imager, along with both the NIRSpec and MRS spectrometers (**Hinkley2019**). Using the MRS, VHS-1256b will be observed using a SLOW readout pattern, using 30 groups per integration, with one integration per exposure using a 2 point dither pattern. This results in a total exposure time of 1433.395s in each of the MRS sub-bands, and will cover the full wavelength range of the MRS. It will be simultaneously imaged using the MIRIM instrument. An additional background only exposure will be taken using the same exposure parameters, but without dithering, for a total of half of the science exposure time.

Methane spectral features have been detected in the L-band spectrum of VHS-1256b (Miles et al., 2018), but mid infrared spectroscopy will allow the use of methane and other molecules to characterize atmospheric properties such as dis-equilibrium chemistry and vertical mixing (Charles A Beichman et al., 2019c).

2M1207b

2M1207b is a 1600K, 10 M_{Jup} object at wide separation from its brown dwarf primary (TWA 27) and a distance of 52.4pc (Bowler, 2016). In comparison to VHS-1256b, 2M1207b has a relatively small separation of 0.77", which is more characteristic of currently known objects. As one of the first directly imaged exoplanets, it provides a template for characterizing young, hot objects, and will be observed in the JWST GTO program 1270 (**Birkmann2019**). This observation will use the NIRSpec IFU, MIRIM and the MIRI MRS.

Using the MRS, 2M1207b will be observed using a FAST readout to prevent detector saturation, using 76 groups per integration, and one integration per exposure. It will use a 4 exposure dither pattern, for a total integration time of 843.612s per sub-band, covering the full wavelength range of the MRS. Combined with the NIRSpec observation, this will provide a continuous spectrum over the entire JWST wavelength range. The host star of 2M1207b is faint, allowing for good enough contrast for a straightforward observation (Charles A Beichman et al., 2019c).

WISE 0855-0714

Although it is a Y-type brown dwarf, WISE 0855 is the most similar known object to Jupiter outside our solar system that has been directly observed (Luhman, 2014). At 250K, WISE 0855 is very faint, with an H-band magnitude of 25, but its proximity at 2pc makes it an ideal target for characterization. The JWST GTO Program 1230 will observe WISE 0855 using NIRCam, NIRSpec and the MIRI MRS (**Oliveira2019**). It will use a FAST readout, with 180 groups per integration, and one integration per exposure for a total of 999s of integration time for each sub-band. No dithering will be used.

As a cold object, WISE 0855 provides the best known extra-solar template for older planetary mass objects. With the improved sensitivity and long wavelength coverage of JWST, it is hoped that more low mass and colder exoplanets may be directly imaged. Understanding the atmosphere of WISE 0855 will provide a great deal of insight for the challenges of such exoplanetary atmospheres. Clouds are suspected to be present (Jacqueline K Faherty et al., 2018), a feature which will be better understood using mid infrared observations.

Science Goals

Atmospheric retrievals are currently the best tools for characterizing the composition and structure of exoplanet atmospheres. Parameters such as the C/O ratio may trace the formation history of planets, and may be able to settle the debate between gravitational instability and core accretion formation models (Nikku Madhusudhan, 2012; Moses et al., 2013). From solar system observations, along with our own experience on Earth, we know atmospheres are constantly changing, and time series observations will open the door to investigation of dynamics and variability. Understanding the composition and chemistry of these atmospheres will also provide insight into the diversity - and similarity - between these systems. Clouds are poorly understood within our own solar system, and are certain to be present in the atmospheres of other worlds. Perhaps the most interesting prospect is uncovering novel features that have not yet been predicted, and will open the door to new avenues of exploration.

For this work, we are primarily concerned with constraining the ability of the MRS to retrieve known input parameters. With simulated spectra from petitRADTRANS providing a ground truth, we can compare the results of retrievals over a range of fringing cases.

4.4 METHODS

Here we will outline how we generated our input spectra, and the procedure we used to perform our atmospheric retrieval.

4.4.1 Spectra Generation

We used petitRADTRANS in high resolution, line-by-line mode in order to calculate a spectrum that can be passed as input to MIRISIM. The parameters chosen for each target are given in table 6. All spectra cover a range of 4.8-18.5 micron in order to fully cover channels 1 through 3 of the MRS. Channel 4 is ignored due to photometric calibration issues.

The spectra generated by petitRADTRANS are in terms of the emitted flux and are in units of erg cm^{-2} m^{-2} s^{-1} Hz^{-1}. MIRISIM requires the flux incident on the detector in units of μJy, so we convert the as

$$F_{inc}[\mu\text{Jy}] = 10^{29} \times F_{em} \times \left(\frac{R_{pl}}{d_{pl}}\right)^2 \tag{12}$$

The wavelength grid produced by petitRADTRANS is logspaced, and we use the `spectres` python package (Carnall, 2017) in order to convert to a linear spaced grid with R=30000 at 4.8μm. This ensures the input spectrum will greatly oversample the instrumental spectral resolution.

While it is possible to add a background term to a spectrum using MIRISIM, we chose not to use any background in order to improve our spectral extraction after processing with the JWST pipeline, with the understanding that errors from background subtraction will be negligible in actual data.

Parameter	**VHS-1256b**	**2M1207b**	**WISE 0855**
Radius [R_{Jup}]	1.29	1.5	1
Distance [pc]	12.7	52.4	2.23
$\log g$	4.25	3.2	4
T_{int} [K]	900	1600	250
T_{equ} [K]	3.4	10	3.4
κ_{IR}	0.01	0.01	0.01
γ	0.3	0.4	0.3
Abundances			
H_2	0.898	0.74	0.73
He	0.102	0.24	0.25
H_2O	1×10^{-3}	5×10^{-3}	5×10^{-4}
CO	1×10^{-7}	1×10^{-2}	1×10^{-15}
CO_2	1×10^{-5}	1×10^{-3}	1×10^{-14}
CH_4	3×10^{-3}	1×10^{-6}	3×10^{-4}
NH_3	1×10^{-5}	1×10^{-7}	3×10^{-3}
C_2H_2	1×10^{-8}	1×10^{-9}	...
HCN	1×10^{-10}	1×10^{-9}	1×10^{-9}
TiO	...	5×10^{-7}	...
SiO	1×10^{-6}	...	...

Table 6: Input parameters to generate spectra using petitRADTRANS. High resolution line-by-line mode was used. κ_{IR} and γ are the infrared opacity and ratio of visible to IR opacities respectively. The values chosen for these parameters are based on (P. Mollière et al., 2019). The abundances chosen are arbitrary values chosen to encompass a wide range of compositions and to test the ability of the retrieval code to recover small abundances. Where possible, values were chosen to qualitatively reflect known species present (Miles et al., 2018).

Figure 11: Bayesian evidence for models of differing dimensionality.

4.4.2 Atmospheric Retrieval Setup

Prior choice

4.5 RESULTS

4.5.1 Model Selection

4.5.2 Fringing Comparison

Figure 12: Posterior Distributions for XX for different fringe cases

Parameter	Prior	Constraints
$\log\delta$	$\mathcal{N}(-5.5, 2.5)$	
$\log\gamma$	$\mathcal{N}(0, 2)$	
T_{int}	$\mathcal{U}(0, 3500)$	
T_{equ}	$\mathcal{U}(0, 30)$	
$\log P_{Trans}$	$\mathcal{N}(-3, 3)$	
α	$\mathcal{N}(0.25, 0.4)$	$\alpha < 1$
$\log g$	$\mathcal{U}(2.0, 4.5)$	
$\log P_0$	$\mathcal{U}(-5, 2)$	
$\ln(X_i)$	$\mathcal{U}(-18, 0)$	$\sum X_i < 1$

Table 7: Prior choices for atmospheric retrievals. $\mathcal{U}(a, b)$ is a uniform distribution from a to b. $\mathcal{N}(\mu, \sigma)$ is a normal distribution. T_{int} corresponds to the effective temperature of an object, while T_{equ} is the equilibrium temperature between an object and a host star. For free floating objects, T_{equ} is set to 3.4K, justifying the small range of the prior. δ is in units of bar^{-1}, temperatures are in K, and pressures in bar.

Figure 13: Posterior Distributions for

4.5.3 VHS-1256b

4.5.4 2M1207b

4.5.5 WISE 0855

Figure 14: Pressure Temperature profile for

Figure 15: Best fit model for

Figure 16: Posterior Distributions for

Figure 17: Pressure Temperature profile for

Figure 18: Best fit model for

Figure 19: Posterior Distributions for

Figure 20: Pressure Temperature profile for

Figure 21: Best fit model for

5 | DISCUSSION AND CONCLUSIONS

A APPENDICES

A.1 PACKAGE REQUIREMENTS

```
numpy=1.4.0
scipy=1.5
```

WORKS CITED

Ackerman, Andrew S. and Mark S. Marley. "Precipitating condensation clouds in substellar atmospheres". *Astrophysical Journal* 596. ISSN: 15384357. DOI: 10.1088/0004-637X/765/1/75 (2001): 872–885. Print.

Aoyama, Yuhiko and Masahiro Ikoma. "Constraining Planetary Gas Accretion Rate from H α Linewidth and Intensity: Case of PDS 70 b and c". *arXiv eprint*. arXiv: arXiv:1909.08175v2 (2019). arXiv: arXiv:1909.08175v2. arXiv: arXiv:1909.08175v2.

Argyriou, Ioannis, Ruymán Azzollini, and Bart Vandenbussche. "Spectrum extraction from detector plane images for the medium-resolution spectrometer of the mid-Infrared Instrument on-board the James Webb Space Telescope." *SPIE*. 2018. 124. Print.

Argyriou, Ioannis, Bart Vandenbussche, and Martyn Wells. "Fringing solution for the mid-infrared instrument on-board the James Webb Space Telescope". *SPIE*. 2018. 127. Print.

Argyriou, Ioannis, et al. "Nature of point source fringes in mid-infrared spectra acquired with the James Webb Space Telescope". *Astronomy & Astrophysics* (): 1–13. Print.

Barman, Travis S., Quinn M. Konopacky, Bruce Macintosh, and Christian Marois. "Simultaneous detection of water, methane, and carbon monoxide in the atmosphere of Exoplanet hr 8799 b". *Astrophysical Journal* 804.1. ISSN: 15384357. DOI: 10.1088/0004-637X/804/1/61. arXiv: 1503.03539 (2015): 1–10. arXiv: 1503.03539. arXiv: 1503.03539. Web. <http://dx.doi.org/10.1088/0004-637X/804/1/61>.

Batalha, Natasha E., et al. " Strategies for Constraining the Atmospheres of Temperate Terrestrial Planets with JWST ". *The Astrophysical Journal* 856.2. ISSN: 2041-8213. DOI: 10.3847/2041-8213/aab896. arXiv: 1803.07983 (2018): L34. arXiv: 1803.07983. arXiv: 1803.07983. Web. <http://dx.doi.org/10.3847/2041-8213/aab896>.

Baudino, Jean-loup, et al. "Toward the Analysis of JWST Exoplanet Spectra : Identifying Troublesome Model Parameters". *The Astrophysical Journal* 850.2. ISSN: 1538-4357. DOI: 10.3847/1538-4357/aa95be (2017): 150. Web. <http://dx.doi.org/10.3847/1538-4357/aa95be>.

Beamín, J. C., et al. "Temperature constraints on the coldest brown dwarf known: WISE 0855-0714". *Astronomy and Astrophysics* 570. ISSN: 14320746. DOI: 10.1051/0004-6361/201424505 (2014): 1–4. Print.

Behmard, Aida, Erik A. Petigura, and Andrew W. Howard. "Data-driven Spectroscopy of Cool Stars at High Spectral Resolution". *The Astrophysical Journal* 876.1. DOI: 10.3847/1538-4357/ab14e0. arXiv: arXiv:1904.00094v1 (2019): 68. arXiv: arXiv:1904.00094v1. arXiv: arXiv:1904.00094v1.

Beichman, Charles A., Pierre-olivier Lagage, and Marie Ygouf. "1188 - Spectroscopy of Young , Widely Separated Exoplanets". 4. Print.

Beichman, Charles A., et al. "1194 - Characterization of the HR 8799 planetary system and planet search". Print.

Beichman, Charles A and Thomas P Greene. "Observing Exoplanets with the James Webb Space Telescope". *Handbook of Exoplanets* 2009. DOI: 10.1007/978-3-319-55333-7_85 (2018): 1283–1308. Print.

Benneke, Bjoern and Sara Seager. "Atmospheric retrieval for super-earths: Uniquely constraining the atmospheric composition with transmission spectroscopy". *Astrophysical Journal* 753.2. ISSN: 15384357. DOI: 10.1088/0004-637X/753/2/100. arXiv: 1203.4018 (2012). arXiv: 1203.4018. arXiv: 1203.4018.

Benneke, Björn. "Bayesian Atmospheric Retrieval for Exoplanets". Diss. Massachusetts Institute of Technology, 2013. Print.

Biller, Beth. "The time domain for brown dwarfs and directly imaged giant exoplanets: the power of variability monitoring". *Astronomical Review* 13.1. ISSN: 2167-2857. DOI: 10.1080/21672857.2017.1303105 (2017): 1–27. Web. <http://dx.doi.org/10.1080/21672857.2017.1303105>.

Biller, Beth A. and Mickaël Bonnefoy. "Exoplanet Atmosphere Measurements from Direct Imaging". *Handbook of Exoplanets*. DOI: 10.1007/978-3-319-55333-7_101. arXiv: arXiv:1807.05136v1 (2018): 2107–2135. arXiv: arXiv:1807.05136v1. arXiv: arXiv:1807.05136v1.

Blanco-Cuaresma, Sergi. "Modern stellar spectroscopy caveats". *Monthly Notices of the Royal Astronomical Society* 486.2. arXiv: arXiv:1902.09558v2 (2019): 2075–2101. arXiv: arXiv:1902.09558v2. arXiv: arXiv:1902.09558v2.

Boccaletti, A., et al. "The Mid-Infrared Instrument for the James Webb Space Telescope , V: Predicted Performance of the MIRI Coronagraphs". *Publications of the Astronomical Society of the Pacific* 127.953. ISSN: 00046280. DOI: 10.1086/682256. arXiv: 1508.02352 (2015): 633–645. arXiv: 1508.02352. arXiv: 1508.02352.

Bodis, Lorant. "Quantification of spectral similarity towards automatic spectra verification". Diss. ETH Zurich, 2007. Web. <https://doi.org/10.3929/ethz-a-005479205>.

Bouchet, Patrice, et al. "The Mid-Infrared Instrument for the James Webb Space Telescope, III: MIRIM, The MIRI Imager". *Publications of the Astronomical Society of the Pacific* 127.953. ISSN: 00046280, 15383873 (2015): 612–622. Web. <http://www.jstor.org/stable/10.1086/682254>.

Bowler, Brendan P. "Imaging Extrasolar Giant Planets". *Publications of the Astronomical Society of the Pacific* 128.968. ISSN: 1538-3873. DOI: 10.1088/1538-3873/128/968/102001 (2016): 1–38. Web. <http://dx.doi.org/10.1088/1538-3873/128/968/102001>.

Bozza, Valerio, Luigi Mancini, and Alessandro Sozzetti. *Astrophysics of Exoplanetary Atmospheres*. Print.

Buchner, J., et al. "X-ray spectral modelling of the AGN obscuring region in the CDFS: Bayesian model selection and catalogue". *Astronomy and Astrophysics* 564. ISSN: 14320746. DOI: 10.1051/0004-6361/201322971. arXiv: 1402.0004 (2014): 1–25. arXiv: 1402.0004. arXiv: 1402.0004.

Buenzli, Esther, et al. "Cloud Structure of the Nearest Brown Dwarfs II: High Amplitude Variability for Luhman 16 A and B In and Out of the 0.99$$m FeH Feature". *Astrophysical Journal* 812.2. ISSN: 15384357. DOI: 10.1088/0004-637X/812/2/163. arXiv: 1509.06148 (2015). arXiv: 1509.06148. arXiv: 1509.06148.

Buenzli, Esther, et al. "Cloud structure of the nearest brown dwarfs: Spectroscopic variability of Luhman 16AB from the Hubble space telescope". *Astrophysical Journal* 798.2. ISSN: 15384357. DOI: 10.1088/0004-637X/798/2/127. arXiv: 1411.0003 (2015). arXiv: 1411.0003. arXiv: 1411.0003.

Burrows, Adam, David Sudarsky, and Jonathan I. Lunine. "Beyond the T Dwarfs: Theoretical Spectra, Colors, and Detectability of the Coolest Brown Dwarfs". *The Astrophysical Journal* 596. DOI: 10.1086/377709. arXiv: arXiv:1306.2144v2 (2003): 587–596. arXiv: arXiv:1306.2144v2. arXiv: arXiv:1306.2144v2. Web. <http://dx.doi.org/10.3847/0004-6256/152/6/217>.

Bushouse, Howard, Michael Droettboom, and Perry Greenfield. "The James Webb Space Telescope Data Calibration Pipeline". *14th Python in Science Conf*. 2015. 289. arXiv: 0606175 [astro-ph].

Chauvin, G., et al. "A giant planet candidate near a young brown dwarf Direct VLT/NACO observations using IR wavefront sensing". *Astronomy and Astrophysics* 425.2. ISSN: 00046361. DOI: 10.1051/0004-6361:200400056 (2004): 29–32. Print.

Chauvin, G., et al. "Orbital characterization of the β Pictoris b giant planet". *Astronomy and Astrophysics* 542. ISSN: 00046361. DOI: 10.1051/0004-6361/201118346. arXiv: 1202.2655 (2012): 1–9. arXiv: 1202.2655. arXiv: 1202.2655.

Chen, Howard, Eric T. Wolf, Zhuchang Zhan, and Daniel E. Horton. "Habitability and Spectroscopic Observability of Warm M-dwarf Exoplanets Evaluated with a 3D Chemistry-Climate Model". arXiv: 1907.10048 (2019). arXiv: 1907.10048. arXiv: 1907.10048. Web. <http://arxiv.org/abs/1907.10048>.

Chilcote, Jeffrey, et al. " 1–2.4 μ m Near-IR Spectrum of the Giant Planet β Pictoris b Obtained with the Gemini Planet Imager ". *The Astronomical Journal* 153.4. ISSN: 0004-6256. DOI: 10.3847/1538-3881/aa63e9. arXiv: 1703.00011 (2017): 182. arXiv: 1703.00011. arXiv: 1703.00011. Web. <http://dx.doi.org/10.3847/1538-3881/aa63e9>.

Chilcote, Jeffrey, et al. "The first H-band spectrum of the giant planet β Pictoris b". *Astrophysical Journal Letters* 798.1. ISSN: 20418213. DOI: 10.1088/2041-8205/798/1/L3 (2015): 1–5. Print.

Christiaens, Valentin, et al. "Evidence for a Circumplanetary Disk around Protoplanet PDS 70 b". *The Astrophysical Journal* 877.2. ISSN: 2041-8213. DOI: 10.3847/2041-8213/ab212b. arXiv: 1905.06370 (2019): L33. arXiv: 1905.06370. arXiv: 1905.06370. Web. <http://dx.doi.org/10.3847/2041-8213/ab212b>.

Consortium, Miri European. "MIRISim Documentation" (2018). Print.

Cooper, Curtis S, David Sudarsky, John A Milsom, and Jonathan I Lunine. "Modeling the Formation of Clouds in Brown Dwarf Atmospheres". *The Astrophysical Journal* 156.2. DOI: 10.1086/367763. arXiv: 0205192v3 [arXiv:astro-ph] (2003): 1320–1337. arXiv: 0205192v3 [arXiv:astro-ph]. arXiv: 0205192v3 [arXiv:astro-ph].

Cossou, Christophe. "MIRISim Spreadsheet and Quick examples" (2018): 1–12. Print.

Danielski, Camilla, et al. " Atmospheric Characterization of Directly Imaged Exoplanets with JWST /MIRI ". *The Astronomical Journal* 156.6. ISSN: 1538-3881. DOI: 10.3847/1538-3881/aae651. arXiv: 1810.00894 (2018): 276. arXiv: 1810.00894. arXiv: 1810.00894.

De Rosa, Robert J., et al. "Spectroscopic characterization of HD 95086 b with the Gemini Planet Imager". *The Astrophysical Journal* 824.2. ISSN: 1538-4357. DOI: 10.3847/0004-637x/824/2/121. arXiv: 1604.01411 (2016): 121. arXiv: 1604.01411. arXiv: 1604.01411. Web. <http://dx.doi.org/10.3847/0004-637X/824/2/121>.

Faherty, Jacqueline K., et al. "Signatures of cloud, temperature, and gravity from spectra of the closest brown dwarfs". *Astrophysical Journal* 790.2. ISSN: 15384357. DOI: 10.1088/0004-637X/790/2/90 (2014). Print.

Faherty, Jacqueline K, C G Tinney, Andrew Skemer, and Andrew J Monson. "Indications of water clouds in the coldest known brown dwarf". *The Astrophysical Journal Letters* 793.1. arXiv: arXiv:1408.4671v2 (2018). arXiv: arXiv:1408.4671v2. arXiv: arXiv:1408.4671v2.

Fegley, Bruce and Katharina Lodders. "Chemical Models of the Deep Atmospheres of Jupiter and Saturn". *Icarus* 110 (1994): 117–154. Print.

Feng, Y. Katherina, et al. "Characterizing Earth Analogs in Reflected Light: Atmospheric Retrieval Studies for Future Space Telescopes". *The Astronomical Journal* 155.5. ISSN: 1538-3881. DOI: 10.3847/1538-3881/aab95c (2018): 200. Web. <http://dx.doi.org/10.3847/1538-3881/aab95c>.

Feroz, F. and M. P. Hobson. "Multimodal nested sampling: An efficient and robust alternative to Markov Chain Monte Carlo methods for astronomical data analyses". *Monthly Notices of the Royal Astronomical Society* 384.2. ISSN: 00358711. DOI: 10.1111/j.1365-2966.2007.12353.x. arXiv: 0704.3704 (2008): 449–463. arXiv: 0704.3704. arXiv: 0704.3704.

Feroz, F., M. P. Hobson, and M. Bridges. "MultiNest: An efficient and robust Bayesian inference tool for cosmology and particle physics". *Monthly Notices of the Royal Astronomical Society* 398.4. ISSN: 00358711. DOI: 10.1111/j.1365-2966.2009.14548.x. arXiv: 0809.3437 (2009): 1601–1614. arXiv: 0809.3437. arXiv: 0809.3437.

Feroz, Farhan, Michael P. Hobson, Ewan Cameron, and Anthony N. Pettitt. "Importance Nested Sampling and the MultiNest Algorithm". *The Open Journal of Astrophysics* 2.1. DOI: 10.21105/astro.1306.2144. arXiv: 1306.2144 (2019): 1–17. arXiv: 1306.2144. arXiv: 1306.2144.

Fisher, Chloe, et al. "Interpreting High-Resolution Spectroscopy of Exoplanets Using Cross-Correlations and Supervised Machine Learning". arXiv: 1910.11627 (2019): 1–15. arXiv: 1910.11627. arXiv: 1910.11627. Web. <http://arxiv.org/abs/1910.11627>.

Foreman-Mackey, Daniel, David W. Hogg, Dustin Lang, and Jonathan Goodman. "emcee : The MCMC Hammer ". *Publications of the Astronomical Society of the Pacific* 125.925. ISSN: 00046280. DOI: 10.1086/670067. arXiv: 1202.3665 (2013): 306–312. arXiv: 1202.3665. arXiv: 1202.3665.

Gandhi, Siddharth and Nikku Madhusudhan. "Retrieval of exoplanet emission spectra with HyDRA". *Monthly Notices of the Royal Astronomical Soci-*

ety 474.1. ISSN: 13652966. DOI: 10.1093/mnras/stx2748. arXiv: 1710.06433 (2018): 271–278. arXiv: 1710.06433. arXiv: 1710.06433.

Garcia, E. Victor, et al. "Individual, Model-independent Masses of the Closest Known Brown Dwarf Binary to the Sun". *The Astrophysical Journal* 846.2. ISSN: 1538-4357. DOI: 10.3847/1538-4357/aa844f. arXiv: 1708.02714 (2017): 97. arXiv: 1708.02714. arXiv: 1708.02714.

Garland, R. and P. G. J. Irwin. "Effectively Calculating Gaseous Absorption in Radiative Transfer Models of Exoplanetary and Brown Dwarf Atmospheres". March. arXiv: 1903.03997 (2019). arXiv: 1903.03997. arXiv: 1903.03997. Web. <http://arxiv.org/abs/1903.03997>.

Gauza, Bartosz, et al. "Discovery of a young planetary mass companion to the nearby M dwarf VHS J125601.92-125723.9". *Astrophysical Journal* 804.2. ISSN: 15384357. DOI: 10.1088/0004-637X/804/2/96. arXiv: 1505.00806 (2015). arXiv: 1505.00806. arXiv: 1505.00806.

——."Discovery of a young planetary mass companion to the nearby M dwarf VHS J125601.92-125723.9". *Astrophysical Journal* 804.2. ISSN: 15384357. DOI: 10.1088/0004-637X/804/2/96. arXiv: 1505.00806 (2015): 1–18. arXiv: 1505.00806. arXiv: 1505.00806. Web. <http://dx.doi.org/10.1088/0004-637X/804/2/96>.

Glasse, Alistair, et al. "The Mid-Infrared Instrument for the James Webb Space Telescope , IX: Predicted Sensitivity". *Publications of the Astronomical Society of the Pacific* 127.953. ISSN: 00046280. DOI: 10.1086/682259. arXiv: 1508.02427 (2015): 686–695. arXiv: 1508.02427. arXiv: 1508.02427.

Goody, Richard, Robert West, Luke Chen, and David Crisp. "The correlated-k method for radiation calculations in nonhomogeneous atmospheres". *Journal of Quantitative Spectroscopy and Radiative Transfer* 42.6. ISSN: 00224073. DOI: 10.1016/0022-4073(89)90044-7 (1989): 539–550. Print.

Gordon, I. E., et al. "The HITRAN2016 molecular spectroscopic database". *Journal of Quantitative Spectroscopy and Radiative Transfer* 203. ISSN: 00224073. DOI: 10.1016/j.jqsrt.2017.06.038 (2017): 3–69. Print.

Goyal, Jayesh M., et al. "Fully scalable forward model grid of exoplanet transmission spectra". *Monthly Notices of the Royal Astronomical Society* 482.4. ISSN: 13652966. DOI: 10.1093/mnras/sty3001. arXiv: 1810.12971 (2019): 4503–4513. arXiv: 1810.12971. arXiv: 1810.12971.

GRAVITY Collaboration, et al. "Peering into the formation history of beta Pictoris b with VLTI/GRAVITY long baseline interferometry". *Astronomy & Astrophysics* 633. DOI: 10.1051/0004-6361/201936898. arXiv: 1912.04651 (2020): 1–21. arXiv: 1912.04651. arXiv: 1912.04651. Web. <http://arxiv.org/abs/1912.04651>.

Greenbaum, Alexandra Z., et al. "GPI Spectra of HR 8799 c, d, and e from 1.5 to 2.4 μm with KLIP Forward Modeling". *The Astronomical Journal* 155.6. ISSN: 0004-6256. DOI: 10.3847/1538-3881/aabcb8. arXiv: 1804.07774 (2018): 226. arXiv: 1804.07774. arXiv: 1804.07774.

Guillot, T. "On the radiative equilibrium of irradiated planetary atmospheres". *Astronomy and Astrophysics* 520.18. ISSN: 00046361. DOI: 10.1051/0004-6361/200913396. arXiv: 1006.4702 (2010): 1–13. arXiv: 1006.4702. arXiv: 1006.4702.

Haffert, S. Y., et al. "Two accreting protoplanets around the young star PDS 70". *Nature Astronomy* 3.8. ISSN: 23973366. DOI: 10.1038/s41550-019-0780-

5 (2019): 749–754. Web. <http://dx.doi.org/10.1038/s41550-019-0780-5>.

Helling, Christiane and Sarah Casewell. "Atmospheres of Brown Dwarfs". *The Astronomy and Astrophysics Review* 22. arXiv: arXiv:1410.6029v2 (2014): 1–53. arXiv: arXiv:1410.6029v2. arXiv: arXiv:1410.6029v2.

Hoeijmakers, H. J., et al. "Medium-resolution integral-field spectroscopy for high-contrast exoplanet imaging: Molecule maps of the β Pictoris system with SINFONI". *Astronomy and Astrophysics* 617. ISSN: 14320746. DOI: 10.1051/0004-6361/201832902. arXiv: 1802.09721 (2018): 1–11. arXiv: 1802.09721. arXiv: 1802.09721.

Irwin, P. G.J., et al. "The NEMESIS planetary atmosphere radiative transfer and retrieval tool". *Journal of Quantitative Spectroscopy and Radiative Transfer* 109.6. ISSN: 00224073. DOI: 10.1016/j.jqsrt.2007.11.006 (2008): 1136–1150. Print.

Keppler, M., et al. "Discovery of a planetary-mass companion within the gap of the transition disk around PDS 70". *Astronomy and Astrophysics* 617. ISSN: 14320746. DOI: 10.1051/0004-6361/201832957. arXiv: 1806.11568 (2018): 1–21. arXiv: 1806.11568. arXiv: 1806.11568.

Konopacky, Quinn M., Travis S. Barman, Bruce A. Macintosh, and Christian Marois. "Detection of carbon monoxide and water absorption lines in an exoplanet atmosphere". *Science* 339.6126. ISSN: 10959203. DOI: 10.1126/science.1232003 (2013): 1398–1401. Print.

Kreidberg, Laura. "Exoplanet Atmosphere Measurements from Transmission Spectroscopy and Other Planet Star Combined Light Observations". *Handbook of Exoplanets*. DOI: 10.1007/978-3-319-55333-7_100. arXiv: arXiv:1709.05941v2 (2018): 2083–2105. arXiv: arXiv:1709.05941v2. arXiv: arXiv:1709.05941v2.

Labiano-Ortega, Alvaro, et al. "The MIRI Medium Resolution Spectrometer calibration pipeline". exposure 1. DOI: 10.1117/12.2232554 (2016): 117. Print.

Lacis, A. A. and V. Oinas. "A description of the correlated k distribution method for modeling nongray gaseous absorption, thermal emission, and multiple scattering in vertically inhomogeneous atmospheres". *Journal of Geophysical Research* 96.D5. ISSN: 01480227. DOI: 10.1029/90JD01945 (1991): 9027–9063. Print.

Lacour, S., et al. "First direct detection of an exoplanet by optical interferometry". *Astronomy & Astrophysics* 623. ISSN: 0004-6361. DOI: 10.1051/0004-6361/201935253 (2019): L11. Print.

Lafrenière, David, Christian Marois, René Doyon, and Travis Barman. "HST/nicmos detection of HR 8799 B in 1998". *Astrophysical Journal* 694.2. ISSN: 15384357. DOI: 10.1088/0004-637X/694/2/L148 (2009): 148–152. Print.

Lagage, Pierre-olivier and David Barrado. "1278 - MIRI Spectroscopic Observations of Brown Dwarfs". Print.

Lagage, Pierre-olivier, J. Bouwman, and Fred Lahuis. "1275 - Spectroscopic characterization of PSO J318". Print.

Lagage, Pierre-olivier and Thomas L Roellig. "1276 - Spectroscopic Observations of WD 0806-661B". Print.

Lagage, P, et al. "The Mid-Infrared Instrument for the James Webb Space Telescope , IV : The Low Resolution Spectrometer". *Publications of the Astronomical Society of the Pacific* 127.953. DOI: 10.1086/682255. arXiv: 1512:03000 (2015): 1–23. arXiv: 1512:03000. arXiv: 1512:03000.

Lagrange, A. M., et al. "A probable giant planet imaged in the β Pictoris disk* VLT/NaCo deep L'-band imaging". *Astronomy and Astrophysics* 493.2. ISSN: 00046361. DOI: 10.1051/0004-6361:200811325 (2009): 21–25. Print.

Lagrange, A. M., et al. "Evidence for an additional planet in the β Pictoris system". *Nature Astronomy* 3.12. ISSN: 23973366. DOI: 10.1038/s41550-019-0857-1 (2019): 1135–1142. Web. <http://dx.doi.org/10.1038/s41550-019-0857-1>.

Lahuis, F and A Boogert. "How to Get Rid of Fringes in SIRTF/IRS Data". *SFChem 2002: Chemistry as a Diagnostic of Star Formation*. Waterloo, 2003. 335. Print.

Lavie, Baptiste, et al. " HELIOS–RETRIEVAL: An Open-source, Nested Sampling Atmospheric Retrieval Code; Application to the HR 8799 Exoplanets and Inferred Constraints for Planet Formation ". *The Astronomical Journal* 154.3. ISSN: 0004-6256. DOI: 10.3847/1538-3881/aa7ed8. arXiv: 1610.03216 (2017): 91. arXiv: 1610.03216. arXiv: 1610.03216.

Lee, J. M., L. N. Fletcher, and P. G.J. Irwin. "Optimal estimation retrievals of the atmospheric structure and composition of HD189733b from secondary eclipse spectroscopy". *Monthly Notices of the Royal Astronomical Society* 420.1. ISSN: 00358711. DOI: 10.1111/j.1365-2966.2011.20013.x. arXiv: 1110.2934 (2012): 170–182. arXiv: 1110.2934. arXiv: 1110.2934.

Li, Jianfeng, D. Brynn Hibbert, Stephen Fuller, and Gary Vaughn. "A comparative study of point-to-point algorithms for matching spectra". *Chemometrics and Intelligent Laboratory Systems* 82.1-2 SPEC. ISS. ISSN: 01697439. DOI: 10.1016/j.chemolab.2005.05.015 (2006): 50–58. Print.

Line, Michael R. and Vivien Parmentier. "the Influence of Nonuniform Cloud Cover on Transit Transmission Spectra". *The Astrophysical Journal* 820.1. ISSN: 1538-4357. DOI: 10.3847/0004-637x/820/1/78. arXiv: 1511.09443 (2016): 78. arXiv: 1511.09443. arXiv: 1511.09443. Web. <http://dx.doi.org/10.3847/0004-637X/820/1/78>.

Line, Michael R., et al. "A systematic retrieval analysis of secondary eclipse spectra. I. A comparison of atmospheric retrieval techniques". *Astrophysical Journal* 775.2. ISSN: 15384357. DOI: 10.1088/0004-637X/775/2/137. arXiv: 1304.5561 (2013). arXiv: 1304.5561. arXiv: 1304.5561.

Line, Michael R., et al. "Uniform Atmospheric Retrieval Analysis of Ultracool Dwarfs. I. Characterizing Benchmarks, Gl 570D and HD 3651B". *Astrophysical Journal* 807.2. ISSN: 15384357. DOI: 10.1088/0004-637X/807/2/183. arXiv: 1504.06670 (2015): 183. arXiv: 1504.06670. arXiv: 1504.06670. Web. <http://dx.doi.org/10.1088/0004-637X/807/2/183>.

Line, Michael R., et al. "Uniform Atmospheric Retrieval Analysis of Ultracool Dwarfs. II. Properties of 11 T dwarfs". *The Astrophysical Journal* 848.2. ISSN: 1538-4357. DOI: 10.3847/1538-4357/aa7ff0. arXiv: 1612.02809 (2017): 83. arXiv: 1612.02809. arXiv: 1612.02809.

Luhman, K L. "Discovery of a ~250K Brown Dwarf at 2pc from the Sun". *The Astrophysical Journal Letters* 18. DOI: 10.1088/2041-8205/786/2/L18 (2014): 2–7. Print.

Lupu, Roxana E., et al. "Developing Atmospheric Retrieval Methods for Direct Imaging Spectroscopy of Gas Giants in Reflected Light. I. Methane Abundances and Basic Cloud Properties". *The Astronomical Journal* 152.6. ISSN: 0004-6256. DOI: 10.3847/0004-6256/152/6/217. arXiv: 1604.05370 (2016): 217. arXiv: 1604.05370. arXiv: 1604.05370. Web. <http://dx.doi.org/10.3847/0004-6256/152/6/217>.

MacDonald, Ryan J. and Nikku Madhusudhan. "HD 209458b in new light: evidence of nitrogen chemistry, patchy clouds and sub-solar water". *Monthly Notices of the Royal Astronomical Society* 469.2. ISSN: 0035-8711. DOI: 10.1093/mnras/stx804. arXiv: 1701.01113 (2017): 1979–1996. arXiv: 1701.01113. arXiv: 1701.01113.

Macintosh, B., et al. "Discovery and spectroscopy of the young jovian planet 51 Eri b with the Gemini Planet Imager". *Science* 350.6256. ISSN: 10959203. DOI: 10.1126/science.aac5891 (2015): 64–67. Print.

MacKay, David J.C. *Information Theory, Inference, and Learning Algorithms*. Fourth Edi. Cambridge University Press, 2003. Print.

Madhusudhan, N and S Seager. "A Temperature and Abundance Retrieval Method for Exoplanet Atmospheres". *The Astrophysical Journal* 707.1. DOI: 10.1088/0004-637X/707/1/24. arXiv: arXiv:0910.1347v2 (2009): 24–39. arXiv: arXiv:0910.1347v2. arXiv: arXiv:0910.1347v2.

Madhusudhan, Nikku. "Atmospheric Retrieval of Exoplanets". *Handbook of Exoplanets*. DOI: 10.1007/978-3-319-55333-7_104. arXiv: 1808.04824 (2018): 2153–2182. arXiv: 1808.04824. arXiv: 1808.04824.

—."C/O ratio as a dimension for characterizing exoplanetary atmospheres". *Astrophysical Journal* 758.1. ISSN: 15384357. DOI: 10.1088/0004-637X/758/1/36. arXiv: 1209.2412 (2012). arXiv: 1209.2412. arXiv: 1209.2412.

Madhusudhan, Nikku, Marcelino Agúndez, Julianne I. Moses, and Yongyun Hu. "Exoplanetary Atmospheres—Chemistry, Formation Conditions, and Habitability". *Space Science Reviews* 205.1-4. ISSN: 15729672. DOI: 10.1007/s11214-016-0254-3. arXiv: arXiv:1604.06092v1 (2016): 285–348. arXiv: arXiv:1604.06092v1. arXiv: arXiv:1604.06092v1.

Madhusudhan, Nikku, Heather Knutson, Jonathan J Fortney, and Travis Barman. "Exoplanetary Atmospheres". 2014. arXiv: arXiv:1402.1169v1. arXiv: arXiv:1402.1169v1.

Madhusudhan, Nikku, et al. "High C / O Ratio and Weak Thermal Inversion in the Very Hot Atmosphere of Exoplanet WASP-12b". *Nature* 469.7328. DOI: 10.1038/nature09602. arXiv: arXiv:1012.1603 (2011): 64–67. arXiv: arXiv:1012.1603. arXiv: arXiv:1012.1603.

Malik, Matej, et al. "Helios: an Open-Source, Gpu-Accelerated Radiative Transfer Code for Self-Consistent Exoplanetary Atmospheres". *The Astronomical Journal* 153.2. ISSN: 0004-6256. DOI: 10.3847/1538-3881/153/2/56. arXiv: 1606.05474 (2017): 56. arXiv: 1606.05474. arXiv: 1606.05474. Web. <http://dx.doi.org/10.3847/1538-3881/153/2/56>.

Malik, Matej, et al. " Self-luminous and Irradiated Exoplanetary Atmospheres Explored with HELIOS ". *The Astronomical Journal* 157.5. ISSN: 0004-6256.

DOI: 10.3847/1538-3881/ab1084. arXiv: 1903.06794 (2019): 170. arXiv: 1903.06794. arXiv: 1903.06794. Web. <http://dx.doi.org/10.3847/1538-3881/ab1084>.

Mamajek, Eric E. and Cameron P.M. Bell. "On the age of the β pictoris moving group". *Monthly Notices of the Royal Astronomical Society* 445.3. ISSN: 13652966. DOI: 10.1093/mnras/stu1894 (2014): 2169–2180. Print.

Manjavacas, Elena. "Physical characterization of brown dwarfs". Diss. Ruperto-Carola-University of Heidelberg, 2014. Print.

Marley, M S and T D Robinson. "On the Cool Side : Modeling the Atmospheres of Brown Dwarfs and Giant Planets arXiv : 1410 . 6512v1 [astro-ph . EP] 23 Oct 2014". *Annual Review of Astronomy and Astrophysics* 53. DOI: 10.1146/annurev-astro-082214-122522. arXiv: arXiv:1410.6512v1 (2015): 279–323. arXiv: arXiv:1410.6512v1. arXiv: arXiv:1410.6512v1.

Marois, Christian, Bruce Macintosh, Daniel Nadeau, and David Lafrenie. "Angular Differential Imaging: A Powerful High-Contrast Imaging Technique". *The Astrophysical Journal* 641 (2006): 556–564. Print.

Marois, Christian, et al. "Direct imaging of multiple planets orbiting the star HR 8799". *Science* 322.5906. ISSN: 00368075. DOI: 10.1126/science.1166585. arXiv: 0811.2606 (2008): 1348–1352. arXiv: 0811.2606. arXiv: 0811.2606.

Mayor, M and D Queloz. "A Jupiter-mass companion to a solar-type star". *Nature* 378 (1995): 667–668. Print.

Mesa, D., et al. "VLT/SPHERE exploration of the young multiplanetary system PDS70". *Astronomy and Astrophysics* 632. ISSN: 14320746. DOI: 10.1051/0004-6361/201936764. arXiv: 1910.11169 (2019): 1–12. arXiv: 1910.11169. arXiv: 1910.11169.

Miles, Brittany E., et al. "Methane in Analogs of Young Directly Imaged Exoplanets". *The Astrophysical Journal* 869.1. ISSN: 1538-4357. DOI: 10.3847/1538-4357/aae6cd. arXiv: 1810.04684 (2018): 18. arXiv: 1810.04684. arXiv: 1810.04684. Web. <http://dx.doi.org/10.3847/1538-4357/aae6cd>.

Molliere, P. and I. A.G. Snellen. "Detecting isotopologues in exoplanet atmospheres using ground-based high-dispersion spectroscopy". *Astronomy and Astrophysics* 622. ISSN: 14320746. DOI: 10.1051/0004-6361/201834169. arXiv: 1809.01156 (). arXiv: 1809.01156. arXiv: 1809.01156.

Mollière, P., et al. "Observing transiting planets with JWST: Prime targets and their synthetic spectral observations". *Astronomy and Astrophysics* 600. ISSN: 14320746. DOI: 10.1051/0004-6361/201629800. arXiv: 1611.08608 (2017): 1–23. arXiv: 1611.08608. arXiv: 1611.08608.

Mollière, P., et al. "petitRADTRANS: a Python radiative transfer package for exoplanet characterization and retrieval". *Astronomy & Astrophysics* 627. ISSN: 0004-6361. DOI: 10.1051/0004-6361/201935470. arXiv: 1904.11504 (2019): 1–17. arXiv: 1904.11504. arXiv: 1904.11504. Web. <http://arxiv.org/abs/1904.11504%7B%5C%%7D0Ahttp://dx.doi.org/10.1051/0004-6361/201935470>.

Mollière, P, et al. "Model Atmospheres of Irradiated Exoplanets: The Influence of Stellar Parameters, Metallicity and the C/O Ratio". *The Astrophysical Journal* 813.1. ISSN: 1538-4357. DOI: 10.1088/0004-637X/813/1/47 (2015): 47. Web. <http://dx.doi.org/10.1088/0004-637X/813/1/47>.

Morley, Caroline V., et al. "An L Band Spectrum of the Coldest Brown Dwarf". *The Astrophysical Journal* 858.2. ISSN: 1538-4357. DOI: 10.3847/1538-4357/aabe8b. arXiv: 1804.07771 (2018): 97. arXiv: 1804.07771. arXiv: 1804.07771. Web. <http://dx.doi.org/10.3847/1538-4357/aabe8b>.

Morley, Caroline V., et al. "Water clouds in y dwarfs and exoplanets". *Astrophysical Journal* 787.1. ISSN: 15384357. DOI: 10.1088/0004-637X/787/1/78. arXiv: 1404.0005 (2014). arXiv: 1404.0005. arXiv: 1404.0005.

Moroz, V.I. "On the infrared spectra of Jupiter and Saturn (0.9-2.5um)". *Soviet Astronomy* 5.6 (1962). Print.

Moses, J. I., N. Madhusudhan, C. Visscher, and R. S. Freedman. "Chemical consequences of the C/O ratio on hot jupiters: Examples from WASP-12b, CoRoT-2b, XO-1b, and HD 189733b". *Astrophysical Journal* 763.1. ISSN: 15384357. DOI: 10.1088/0004-637X/763/1/25. arXiv: 1211.2996 (2013). arXiv: 1211.2996. arXiv: 1211.2996.

National Academies of Sciences Engineering and Medicine. *Exoplanet science strategy*. Washington, DC: The National Academies Press, 2018. 1–172. DOI: 10.17226/25187. Print.

Oreshenko, Maria, et al. "Supervised Machine Learning for Inter-comparision of Model Grids of Brown Dwarfs: Application to GJ 570D and the Epsilon Indi B Binary System". *The Astronomical Journal* 159.1. DOI: 10.3847/1538-3881/ab5955. arXiv: arXiv:1910.11795v1 (2020): 15. arXiv: arXiv:1910.11795v1. arXiv: arXiv:1910.11795v1.

Petermann, R. "Atmospheric characterization of terrestrial planets using high-resolution spectroscopy with ELT / METIS A study of Proxima Cen b". Diss. ETH Zurich, 2019. Print.

Quanz, Sascha P., et al. "First results from very large telescope NACO apodizing phase plate: 4 μm images of the exoplanet β Pictoris b". *Astrophysical Journal Letters* 722.1 PART 2. ISSN: 20418213. DOI: 10.1088/2041-8205/722/1/L49 (2010): 49–53. Print.

Ressler, M. E., et al. "The Mid-Infrared Instrument for the James Webb Space Telescope , VIII: The MIRI Focal Plane System". *Publications of the Astronomical Society of the Pacific* 127.953. ISSN: 00046280. DOI: 10.1086/682258 (2015): 675–685. Print.

Rich, Evan A., et al. "Thermal Infrared Imaging and Atmospheric Modeling of VHS J125601.92-125723.9 b: Evidence for Moderately Thick Clouds and Equilibrium Carbon Chemistry in a Hierarchical Triple System." *The Astrophysical Journal* 830.2. ISSN: 1538-4357. DOI: 10.3847/0004-637x/830/2/114. arXiv: 1607.06007 (2016): 114. arXiv: 1607.06007. arXiv: 1607.06007. Web. <http://dx.doi.org/10.3847/0004-637X/830/2/114>.

Rieke, G. H., et al. " The Mid-Infrared Instrument for the James Webb Space Telescope , I: Introduction ". *Publications of the Astronomical Society of the Pacific* 127.953. ISSN: 00046280. DOI: 10.1086/682252 (2015): 584–594. Print.

—."The Mid-Infrared Instrument for the James Webb Space Telescope , I: Introduction". *Publications of the Astronomical Society of the Pacific* 127.953. ISSN: 00046280. DOI: 10.1086/682252 (2015): 584–594. Print.

Rieke, G. H., et al. "The Mid-Infrared Instrument for the James Webb Space Telescope , VII: The MIRI Detectors". *Publications of the Astronomical Society* *of the Pacific* 127.953. ISSN: 00046280. DOI: 10.1086/682257 (2015): 665–674. Print.

Robinson, Tyler D., Karl R. Stapelfeldt, and Mark S. Marley. "Characterizing rocky and gaseous exoplanets with 2m class space-based coronagraphs". *Publications of the Astronomical Society of the Pacific* 128.960. ISSN: 00046280. DOI: 10.1088/1538-3873/128/960/025003 (2016): 1–22. Web. <http://dx.doi.org/10.1088/1538-3873/128/960/025003>.

Rothman, L. S., et al. "HITEMP, the high-temperature molecular spectroscopic database". *Journal of Quantitative Spectroscopy and Radiative Transfer* 111.15. ISSN: 00224073. DOI: 10.1016/j.jqsrt.2010.05.001 (2010): 2139–2150. Web. <http://dx.doi.org/10.1016/j.jqsrt.2010.05.001>.

Rothman, L. S., et al. "The HITRAN2012 molecular spectroscopic database". *Journal of Quantitative Spectroscopy and Radiative Transfer* 130. ISSN: 00224073. DOI: 10.1016/j.jqsrt.2013.07.002 (2013): 4–50. Print.

Sahlmann, J. and P. F. Lazorenko. "Mass ratio of the 2 pc binary brown dwarf LUH 16 and limits on planetary companions from astrometry". *Monthly Notices of the Royal Astronomical Society: Letters* 453.1. ISSN: 17453933. DOI: 10.1093/mnrasl/slv113. arXiv: 1506.07994 (2015): L103–L107. arXiv: 1506.07994. arXiv: 1506.07994.

Schlawin, Everett, et al. " Clear and Cloudy Exoplanet Forecasts for JWST : Maps, Retrieved Composition, and Constraints on Formation with MIRI and NIRCam ". *The Astronomical Journal* 156.1. ISSN: 0004-6256. DOI: 10.3847/1538-3881/aac774. arXiv: 1803.08173 (2018): 40. arXiv: 1803.08173. arXiv: 1803.08173.

Schneider, Adam C., Michael C. Cushing, J. Davy Kirkpatrick, and Christopher R. Gelino. " the Collapse of the Wien Tail in the Coldest Brown Dwarf? Hubble Space Telescope Near-Infrared Photometry of Wise J085510.83–071442.5 ". *The Astrophysical Journal* 823.2. ISSN: 2041-8213. DOI: 10.3847/2041-8205/823/2/l35. arXiv: 1605.05618 (2016): L35. arXiv: 1605.05618. arXiv: 1605.05618. Web. <http://dx.doi.org/10.3847/2041-8205/823/2/L35>.

Simkin, Susan M. "Measurements of Velocity Dispersions and Doppler Shifts from Digitized Optical Spectra". *Astronomy & Astrophysics* 32 (1974): 129–136. Print.

Skemer, Andrew J., et al. "First light LBT AO images of HR 8799 bcde at 1.6 and 3.3 μm: New discrepancies between young planets and old brown dwarfs". *Astrophysical Journal* 753.1. ISSN: 15384357. DOI: 10.1088/0004-637X/753/1/14. arXiv: 1203.2615 (2012). arXiv: 1203.2615. arXiv: 1203.2615.

Skemer, Andrew J., et al. "The First Spectrum of the Coldest Brown Dwarf". *The Astrophysical Journal* 826.2. ISSN: 2041-8213. DOI: 10.3847/2041-8205/826/2/l17. arXiv: 1605.04902 (2016): L17. arXiv: 1605.04902. arXiv: 1605.04902. Web. <http://dx.doi.org/10.3847/2041-8205/826/2/L17>.

Skemer, Andrew J., et al. "The LEECH Exoplanet Imaging Survey: Characterization of the Coldest Directly Imaged Exoplanet, GJ 504 b, and Evidence for Super-Stellar Metallicity". *The Astrophysical Journal* 817.2. ISSN: 1538-4357. DOI: 10.3847/0004-637x/817/2/166. arXiv: 1511.09183 (2016): 166.

arXiv: 1511.09183. arXiv: 1511.09183. Web. <http://dx.doi.org/10.3847/0004-637X/817/2/166>.

Skilling, John. "Nested Sampling". 395.November 2004, DOI: 10.1063/1.1835238 (2004): 395–405. Print.

Snellen, I., et al. "Combining high-dispersion spectroscopy with high contrast imaging: Probing rocky planets around our nearest neighbors". *Astronomy and Astrophysics* 576.3. ISSN: 14320746. DOI: 10.1051/0004-6361/201425018. arXiv: 1503.01136 (2015). arXiv: 1503.01136. arXiv: 1503.01136.

Snellen, Ignas, et al. "The fast spin-rotation of a young extrasolar planet". *Nature* 509.7498. ISSN: 0028-0836, 1476-4687. DOI: 10.1038/nature13253. arXiv: 1404.7506 [astro-ph.EP] (2014): 63–65. arXiv: 1404.7506 [astro-ph.EP]. arXiv: 1404.7506 [astro-ph.EP]. Web. <http://arxiv.org/abs/1404.7506%7B%5C%%7D5Cnhttp://www.arxiv.org/pdf/1404.7506.pdf>.

Soummer, Rémi, et al. "Orbital motion of HR 8799 b, c, d using hubble space telescope data from 1998: Constraints on inclination, eccentricity, and stability". *Astrophysical Journal* 741.1. ISSN: 15384357. DOI: 10.1088/0004-637X/741/1/55. arXiv: 1110.1382 (2011). arXiv: 1110.1382. arXiv: 1110.1382.

Speagle, Joshua S. "dynest: A Dynamic Nested Smpling Package for Estimating Bayesian Posteriors and Evidences". *Monthly Notices of the Royal Astronomical Society* 4. ISSN: 0035-8711. DOI: 10.1093/mnras/staa278 (2020). Print.

——."A Conceptual Introduction to Markov Chain Monte Carlo Methods". arXiv: 1909.12313 (2019). arXiv: 1909.12313. arXiv: 1909.12313. Web. <http://arxiv.org/abs/1909.12313>.

Stone, Jordan M., et al. "Adaptive Optics Imaging of Vhs 1256–1257: a Low Mass Companion To a Brown Dwarf Binary System". *The Astrophysical Journal* 818.1. ISSN: 2041-8213. DOI: 10.3847/2041-8205/818/1/l12 (2016): L12. Web. <http://dx.doi.org/10.3847/2041-8205/818/1/L12>.

Tennyson, Jonathan and Sergei N. Yurchenko. "The ExoMol project: Software for computing large molecular line lists". *International Journal of Quantum Chemistry* 117.2. ISSN: 1097461X. DOI: 10.1002/qua.25190. arXiv: 1607.01220 (2017): 92–103. arXiv: 1607.01220. arXiv: 1607.01220.

Tennyson, Jonathan, et al. "The ExoMol database: Molecular line lists for exoplanet and other hot atmospheres". *Journal of Molecular Spectroscopy* 327. ISSN: 1096083X. DOI: 10.1016/j.jms.2016.05.002. arXiv: 1603.05890 (2016): 73–94. arXiv: 1603.05890. arXiv: 1603.05890. Web. <http://dx.doi.org/10.1016/j.jms.2016.05.002>.

Tinney, C G, et al. "The Luminosities of the Coldest Brown Dwarfs". *The Astrophysical Journal* 39.Luhman. DOI: 10.1088/0004-637X/796/1/39 (2014): 1–13. Print.

Tokunaga, Alan T. "High-Resolution Infrared Spectroscopy of Planetary Atmospheres". *Publications of the Astronomical Society of the Pacific* 95.October (1983): 691–699. Print.

VanderPlas, Jacob T. "Understanding the Lomb–Scargle Periodogram". *The Astrophysical Journal Supplement Series* 236.1. ISSN: 0067-0049. DOI: 10.3847/1538-4365/aab766. arXiv: 1703.09824 (2018): 16. arXiv: 1703.09824. arXiv: 1703.09824. Web. <http://dx.doi.org/10.3847/1538-4365/aab766>.

Waldmann, I. P., et al. "T-REx. II. Retrieval of Emission Spectra". *Astrophysical Journal* 813.1. ISSN: 15384357. DOI: 10.1088/0004-637X/813/1/13. arXiv: 1508.07591 (2015): 13. arXiv: 1508.07591. arXiv: 1508.07591. Web. <http://dx.doi.org/10.1088/0004-637X/813/1/13>.

Waldmann, I. P., et al. "Tau-REx I: A next generation retrieval code for exoplanetary atmospheres". *Astrophysical Journal* 802.2. ISSN: 15384357. DOI: 10.1088/0004-637X/802/2/107. arXiv: 1409.2312 (2015): 107. arXiv: 1409.2312. arXiv: 1409.2312. Web. <http://dx.doi.org/10.1088/0004-637X/802/2/107>.

Wells, Martyn, et al. "The Mid-Infrared Instrument for the James Webb Space Telescope , VI: The Medium Resolution Spectrometer". *Publications of the Astronomical Society of the Pacific* 127.953. ISSN: 00046280. DOI: 10.1086/682281. arXiv: 1508.03070 (2015): 646–664. arXiv: 1508.03070. arXiv: 1508.03070.

Wright, G S, et al. "The Mid-Infrared Instrument for JWST , II : Design and Build". *Publications of the Astronomical Society of the Pacific* 127.953. DOI: 10.1086/682253. arXiv: 1508.02333 (2015): 595. arXiv: 1508.02333. arXiv: 1508.02333.

Yurchenko, Sergei N., Ahmed F. Al-Refaie, and Jonathan Tennyson. "EXO CROSS: A general program for generating spectra from molecular line lists". *Astronomy and Astrophysics* 614. ISSN: 14320746. DOI: 10.1051/0004-6361/201732531. arXiv: 1801.09803 (2018): 1–12. arXiv: 1801.09803. arXiv: 1801.09803.

Zalesky, Joseph A., Michael R. Line, Adam C. Schneider, and Jennifer Patience. "A Uniform Retrieval Analysis of Ultra-cool Dwarfs. III. Properties of Y Dwarfs". *The Astrophysical Journal* 877.1. ISSN: 1538-4357. DOI: 10.3847/1538-4357/ab16db. arXiv: 1903.11658 (2019): 24. arXiv: 1903.11658. arXiv: 1903.11658.

Zhang, Michael, Yayaati Chachan, Eliza M.R. Kempton, and Heather A. Knutson. "Forward modeling and retrievals with PLATON, a fast open-source tool". *Publications of the Astronomical Society of the Pacific* 131.997. ISSN: 00046280. DOI: 10.1088/1538-3873/aaf5ad. arXiv: 1811.11761 (2019). arXiv: 1811.11761. arXiv: 1811.11761.

Zucker, S. "Cross-correlation and maximum-likelihood analysis : a new approach to combining cross-correlation functions 2 F RO M M A X I M U M L I K E L I H O O D T O C R O S S - C O R R E L AT I O N 1292". *Monthly Notices of the Royal Astronomical Society* 342 (2003): 1291–1298. Print.

Zurlo, A., et al. "First light of the VLT planet finder SPHERE: III. New spectrophotometry and astrometry of the HR 8799 exoplanetary system". *Astronomy and Astrophysics* 587. ISSN: 14320746. DOI: 10.1051/0004-6361/201526835. arXiv: 1511.04083 (2016): 1–13. arXiv: 1511.04083. arXiv: 1511.04083.